General Disclaimer

One or more of the Following Statements may affect this Document

- This document has been reproduced from the best copy furnished by the organizational source. It is being released in the interest of making available as much information as possible.

- This document may contain data, which exceeds the sheet parameters. It was furnished in this condition by the organizational source and is the best copy available.

- This document may contain tone-on-tone or color graphs, charts and/or pictures, which have been reproduced in black and white.

- This document is paginated as submitted by the original source.

- Portions of this document are not fully legible due to the historical nature of some of the material. However, it is the best reproduction available from the original submission.

JPL PUBLICATION 77-28

Calibration of Viking Imaging System Pointing, Image Extraction, and Optical Navigation Measure

National Aeronautics and Space Administration

Jet Propulsion Laboratory
California Institute of Technology
Pasadena, California 91103

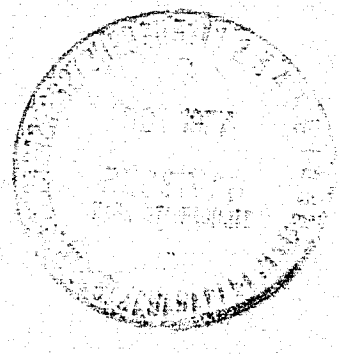

JPL PUBLICATION 77-28

Calibration of Viking Imaging System Pointing, Image Extraction, and Optical Navigation Measure

W. G. Breckenridge and J. W. Fowler
Jet Propulsion Laboratory
E. M. Morgan
General Electric Co.

September 15, 1977

National Aeronautics and
Space Administration

Jet Propulsion Laboratory
California Institute of Technology
Pasadena, California 91103

PREFACE

The work described in this report was performed by the Control and Energy Conversion Division of the Jet Propulsion Laboratory, under the sponsorship of the Viking 1975 Project, managed by Langley Research Center, NASA.

ABSTRACT

The pointing of Viking Orbiter science instruments is controlled by the scan platform. The pointing control and knowledge accuracy required for science and optical navigation data acquisition and evaluation requires calibration of the scan platform and the imaging system. The mathematical models used and the calibration procedure and results obtained for the two Viking spacecraft are described. Included are both ground and in-flight scan platform calibrations, and the additional calibrations unique to optical navigation.

CONTENTS

Figures

Tables

SECTION I

INTRODUCTION

A two-degree-of-freedom scan platform was used to point the Viking Orbiter science instruments. Accurate calibration of platform pointing was required to meet the scientific requirements of the mission. An a priori pointing control accuracy of 0.5 deg (3σ) and an a posteriori knowledge of where the platform had pointed of 0.25 deg (3σ) was desired by the Viking mission.

The experience gained from scan platform calibrations on the Mariner Mars 1969, Mariner Mars 1971, and Mariner Venus/Mercury missions has proven the technique of a two-part calibration, using both ground and in-flight calibration phases.

The ground calibration phase consists of the calibration of the components of the attitude and articulation control systems that affect scan platform pointing and those mechanical alignments that can be easily measured and expected to remain unchanged in flight. The component calibrations most important to accurate platform pointing are the gimbal actuator calibrations. The actuator fine-scale calibration provides the detailed, relative position calibration required to tie together the few points taken during in-flight calibration. The ground calibration results provide the a priori parameter values for the mathematical model of scan platform pointing that is used for determining the commands required to achieve a desired pointing and for reconstruction of the actual pointing from telemetry data.

The in-flight calibration phase provides an end-to-end system calibration that includes errors that could not be measured accurately on the ground, or which were subject to change with the transition from ground to space environment. The in-flight calibration is of sufficient accuracy to assure that mission pointing requirements are met. The in-flight calibration process is an estimation of mathematical model parameters using the difference between the pointing reconstructed from the a priori model and telemetry data and the actual pointing determined from star images appearing in pictures taken by the Viking Imaging System mounted on the scan platform.

The Viking Imaging Systems (VIS) serves several purposes during the mission: the scientific investigation of Mars, imaging stars for in-flight scan platform pointing calibration, and imaging Mars and its satellites with stars for optical navigation. The scan calibration and optical navigation uses of VIS data are closely coupled, using the same processing software, procedures, and personnel; both will be discussed in this report.

The accuracy required for scan platform pointing calibration does not necessitate an accurate calibration of the relative alignment of the two VIS cameras or distortion correction of the VIS pictures. However, the science and optical navigation uses of the VIS data do

require such calibrations, so they are included as part of the in-flight calibration.

The Viking mission is the first to use optical navigation as part of the operational navigation system, and the first to use dual-camera optical measurements. The scan calibration picture sequences provided an opportunity to test and evaluate the optical navigation processing and procedures in a real-time environment prior to the required usage of the system during Mars approach.

All of these diverse but interrelated topics are discussed in this report.

SECTION II

SCAN POINTING SYSTEM

A. DESCRIPTION

The pointing of the scan platform, and the science instruments mounted on it (Figure 2-1), is controlled by two spacecraft subsystems: the attitude control subsystem and the articulation control (ARTC) subsystem. The attitude control subsystem establishes and maintains the spacecraft body attitude relative to celestial references, the Sun and a reference star. The articulation control subsystem controls the two gimbal axes of the scan platform and, thus, the platform's orientation with respect to the spacecraft body. Together, these two subsystems control the scan platform orientation with respect to the celestial references and an inertial coordinate system in which celestial reference directions are defined. The celestial reference, spacecraft, and scan platform coordinate systems are shown in Figure 2-2.

The nominal spacecraft attitude is defined by the directions to the celestial references and the mounting locations of the Sun and star sensors on the spacecraft. The actual spacecraft attitude deviates from nominal within a region defined by the control deadbands. The sensor error signals, which are caused by this deviation, are telemetered to the ground for use in the reconstruction of the spacecraft attitude.

The scan platform clock and cone gimbal axis angles are controlled by digital commands to the ARTC. One of the redundant ARTC channels converts the command to a voltage that is compared to the feedback voltage from the actuator with the difference error signal driving the actuator stepping motor until the null is attained. The actual actuator angle is indicated by telemetered voltage from coarse and fine potentiometers geared to the actuator shaft. A simplified representation of one axis of articulation control is shown in Figure 2-3.

The two cameras of the Viking Imaging System (VIS) are mounted on the scan platform and are offset from the platform MNL coordinate system (Figure 2-2). Instrument offset angles are defined as shown in Figure 2-4.

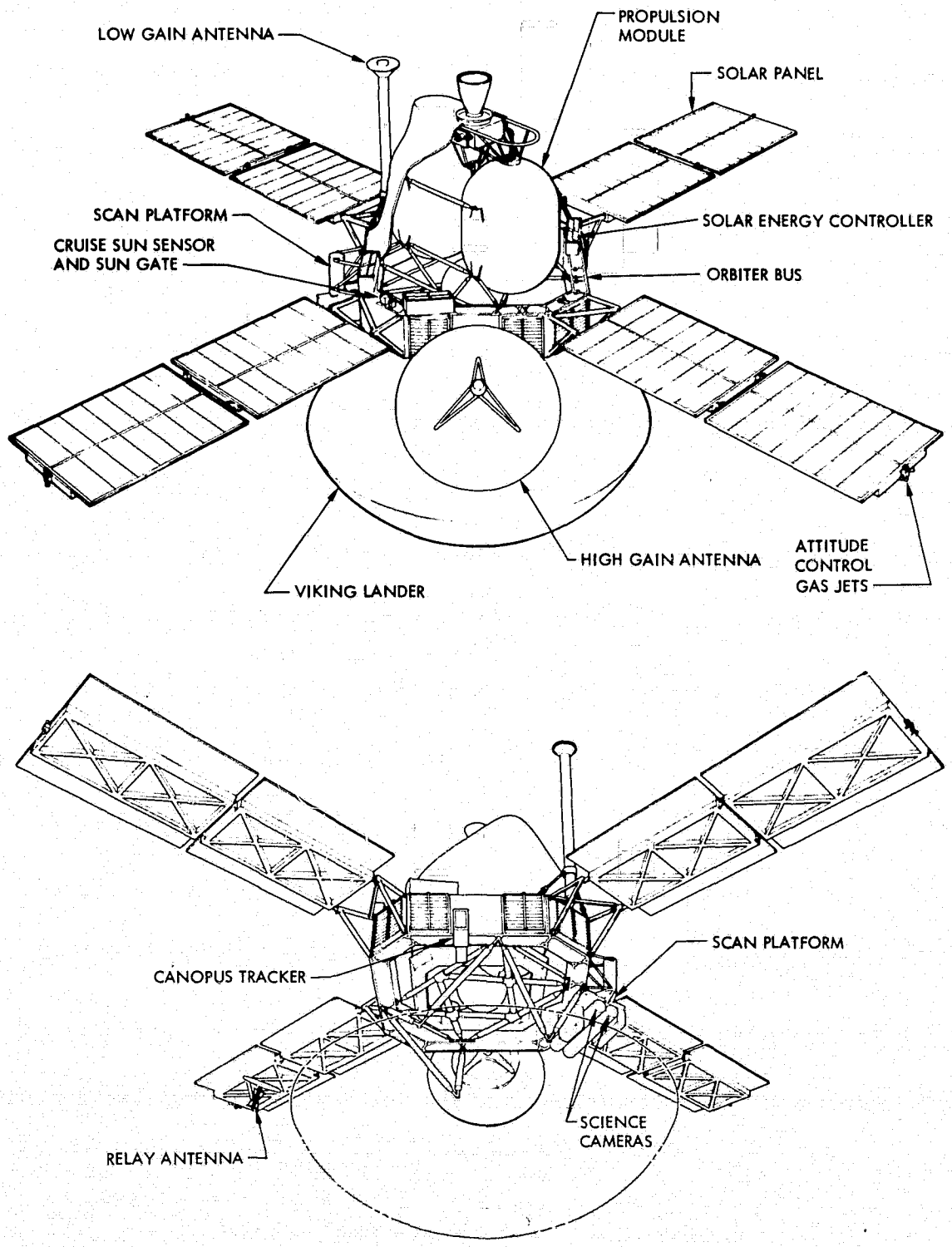

Figure 2-1. Viking Spacecraft

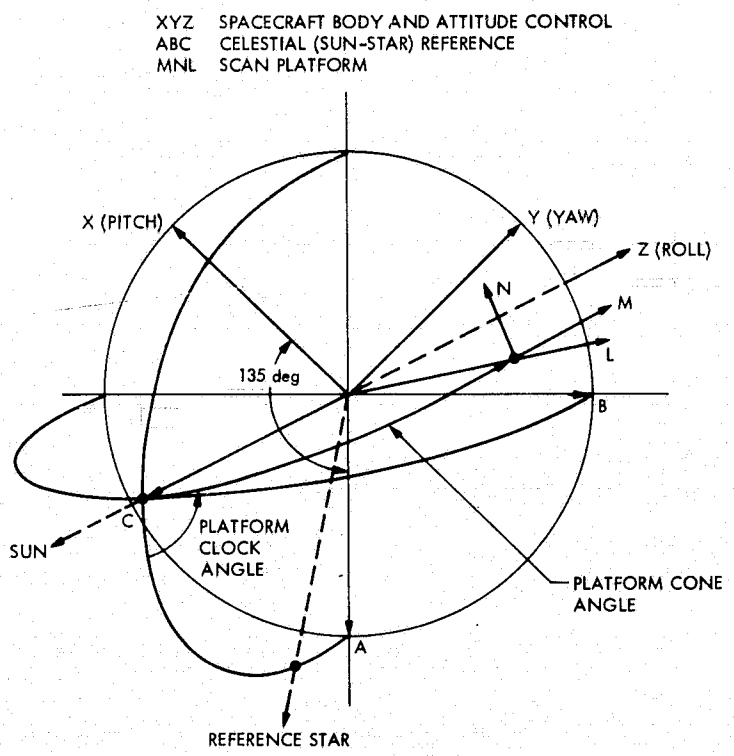

Figure 2-2. Coordinate System Definitions

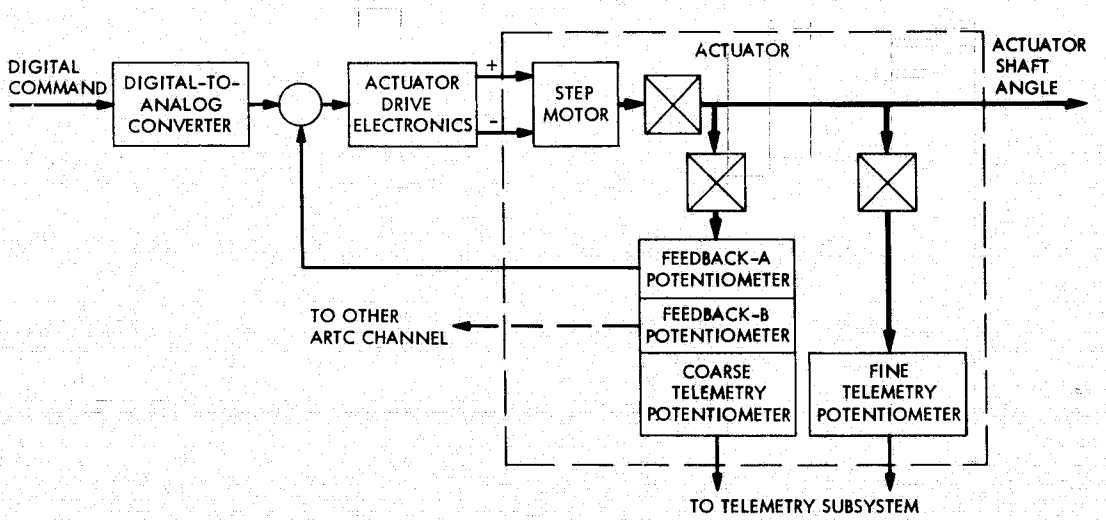

Figure 2-3. One Axis of Articulation Control

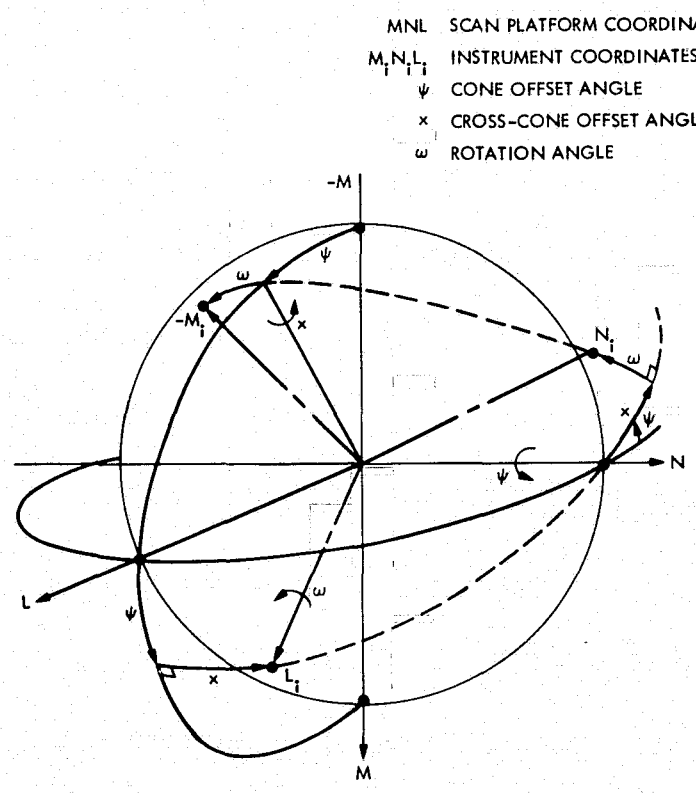

Figure 2-4. Instrument Offset Angles

B. MODELS

The mathematical models used in the various software elements fall into three categories: the nominal model, which defines the spacecraft attitude and scan platform pointing of an error-free system; the articulation control model, which defines the subsystem level performance of the ARTC and is defined by ground calibration; and the error model, which defines the system level deviations of in-flight performance and is evaluated by the in-flight calibration. The nominal model consists of the mathematical relationships between the coordinate systems previously defined in this section. The ARTC model is defined in the next section. The remainder of this section describes the error model components that were evaluated during in-flight calibration.

The attitude control sensor errors are modeled by a null offset, θ_0, and a scale factor correction, k, typically:

$$\theta_{true} = \theta_0 + (1 + k)\theta_{measured}$$

The scan platform structural errors are modeled by five coordinate misalignments (nominal coordinates are shown in Figure 2-2):

(1) Clock gimbal axis misalignment about A-axis.

(2) Clock gimbal axis misalignment about B-axis.

(3) Nonorthogonality of clock and cone gimbal axes.

(4) Nonorthogonality of cone gimbal and L-axis (platform cross-cone error).

(5) Scan Platform (MNL) rotation error about L-axis.

The scan platform gimbal angle error model includes the required corrections to the actuator angle, θ_A, from the ARTC model.

$$\theta = \theta_A + \Delta\theta_A - A_1\theta_A \mp (A_2 \cdot \theta_A + H)$$

where

$\Delta\theta_A$ = gimbal null offset

A_1 = gimbal wind-up error

A_2 = gimbal windup hysteresis error

H = gimbal hysteresis error

$\mp$ = - sign of last angle change of gimbal

The attitude sensor and gimbal actuator angle measurement noise was mainly due to the resolution (7 bits) of the digital telemetry. The noise model uses $\pm 1/2$ DN as the error value for these five angle measurements:

sun sensor (pitch and yaw)	$\pm$0.01 deg
star tracker (roll)	$\pm$0.015 deg
gimbal actuator (clock and cone)	$\pm$0.02 deg

The model of a VIS camera consists of four parts: alignment with respect to the scan platform, the optics relating the imaged scene to the image plane, the raster and distortion model relating picture coordinates to the image plane, and a "standard camera" relating image plane coordinates to pseudo-picture coordinates that are more readily recognized by the analyst using the model.

The alignment of each camera is defined by the three offset angles ψ(cone), χ(cross-cone), and ω(rotation) defined in Figure 2-4.

The optics model relates a vector, V, to an imaged object in VIS MNL coordinates through the focal length, F, of the optics to image plane coordinates (XY, in mm).

$$\begin{bmatrix} X \\ Y \end{bmatrix} = \left(\frac{F}{V_L} \right) \cdot \begin{bmatrix} -V_m \\ +V_n \end{bmatrix}$$

The raster and distortion model transforms from picture line and pixel (L, P) coordinates to the image plane. The following sequence of equations defines the model, where primes indicate intermediate transformations of X and Y.

$$\begin{bmatrix} X''' \\ Y''' \end{bmatrix} = K_{2\times2} \begin{bmatrix} (L - L_0) \\ (P - P_0) \end{bmatrix}$$

where:

(L_0, P_0) = coordinates of picture central rescan

K = scale factor, rotation and nonorthogonality of scan raster (line and pixel to mm units)

$$\begin{bmatrix} X'' \\ Y'' \end{bmatrix} = \frac{1}{1 + P_1X''' + P_2Y'''} \begin{bmatrix} X''' \\ Y''' \end{bmatrix}$$

where:

P_1, P_2 = perspective parameters, for "new" nonparallel scan raster coordinate system error

$$\begin{bmatrix} X' \\ Y' \end{bmatrix} = \begin{bmatrix} X'' \\ Y'' \end{bmatrix} + \begin{bmatrix} \Delta_e & -\Delta_o \\ \Delta_o & \Delta_e \end{bmatrix} \begin{bmatrix} (X'' - X_0) \\ (Y'' - Y_0) \end{bmatrix}$$

where:

$\Delta_e = \Sigma_i \gamma_i r^i \quad i = 2,4,6$ (even, radial error)

$\Delta_o = \Sigma_i \gamma_i r^i \quad i = 1,3,5$ (odd, tangential error)

γ_i = electromagnetic distortion coefficients

$r = ((X'' - X_0)^2 + (Y'' - Y_0)^2)^{1/2}$

(X_o, Y_o) = electromagnetic distortion center

$$\begin{bmatrix} X \\ Y \end{bmatrix} = \begin{bmatrix} X' \\ Y' \end{bmatrix} + \begin{bmatrix} B_1 & B_2 \\ -B_2 & B_1 \end{bmatrix} \begin{bmatrix} x(x^2 - 3y^2) \\ y(y^2 - 3x^2) \end{bmatrix}$$

where:

B_1, B_2 = coefficients of "new" distortion error

$(x, y) = ((X' - X_c), (Y' - Y_c))$

(X_c, Y_c) = center of "new" distortion error

The "standard camera" model is:

$$\begin{bmatrix} L_s \\ P_s \end{bmatrix} = \begin{bmatrix} L_{so} \\ P_{so} \end{bmatrix} + SK_{2\times2} \begin{bmatrix} X \\ Y \end{bmatrix}$$

where:

SK = "standard" raster $\approx K^{-1}$ (mm to l,p)

(L_{s0}, P_{s0}) = "standard" center $\approx (L_0, P_0)$

SECTION III

ARTC GROUND CALIBRATIONS

A. INTRODUCTION

This section of the report defines the mathematical model of the articulation control subsystem that is used in the software for pointing command generation, pointing reconstruction and ARTC calibration. Components modelled are the command digital-to-analog converter (DAC), actuators, and the Flight Data System (FDS) analog-to-digital converters for telemetry. The actuators may be high-gain antenna gimbals or solar energy controllers as well as the scan platform gimbals.

The data, software, and procedure used for DAC and actuator calibrations are described. Typical calibration results are given in terms of the modelling accuracy achieved.

B. ARTC SOFTWARE MODELS

The ARTC calibration may be viewed as a process of applying numerical regression techniques and residual error analysis to data recorded in the laboratory during assembly-level testing of the hardware, where the regression equations are the equations employed in the ARTC software models. These same models are used in the Viking Operations Software requiring an ARTC model. These equations evolved from their original form as the result of the behavioral properties discovered in the lab data. The equations presented in this section are the final form used in the ARTC model and the historical development of the modeling philosophy will not be given here.

The ARTC model is concerned with the following hardware units:

(1) Flight data subsystem (FDS) interface with the ARTC subsystem.

(2) Digital-to-analog converter (DAC).

(3) Actuators for the scan platform clock and cone axes, the high-gain antenna (HGA) azimuth (Az) and elevation (El) axes, and the solar energy controllers (SECs).

The FDS response to a voltage ratio (V) from a telemetry potentiometer (TM pot) in data number (DN) is given by the linear relation

$$V = \alpha + \beta \, DN \qquad (1)$$

where α and β are the regression coefficients for bias and slope, respectively.

The DAC voltage ratio output in response to a command number N is

$$V = V_0 + \sum_{i=1}^{10} N_i \Delta V_i \qquad (2)$$

where V_0 is the residual output voltage ratio (DAC output for N = 0), N_i is the i^{th} binary bit of the ten-binary-bit command N, and V_i is the corresponding voltage ratio increment; the V_i obey the approximate relation

$$\Delta V_i \approx 2^{i-11}$$

The DAC output is modified by a noise model correction,

$$V \longleftarrow V + \Delta V_N$$

where the noise correction ΔV_N is given by

$$\Delta V_N = \rho_1 + \rho_2 V + \rho_3 V^2 \qquad (3)$$

and the regression coefficients ρ_1, ρ_2, ρ_3 are calculated separately for each combination of ARTC Electronics (ARTC-E) channel, slew rate, and slew direction. This appeared necessary early in the assembly-level testing, but when the hardware was put into the flight configuration, it was found that the noise coefficients could be set to zero.

Each actuator contains two feedback potentiometers (FB pots), one for each ARTC-E channel, and a coarse TM pot, all of which have voltage ratio responses V that depend on actuator output shaft angle ϕ according to the linear relation

$$V = A + B\,(\phi - \phi_0) \qquad (4)$$

where A and B are regression coefficients and ϕ_0 is the central angle of the output shaft. The FB pots are also treated for nonlinearity by fitting their deviations from linearity to piece-wise linear fits $\delta V(V)$, where the endpoints of the linear segments are stored in a table $(\delta V_i, V_i)$ in which linear interpolation may be performed.

$$V \longleftarrow V + \delta V(V)$$

$$\phi = \phi_0 + \frac{V - A}{B}$$

Hysteresis corrections to Eq. (4) are provided by hysteresis lookup tables, $\Delta\phi_i(\phi_i)$, for each slew direction, within which hysteresis corrections $\Delta\phi(\phi)$ may be calculated by linear interpolation; then ϕ is corrected by

$$\phi \longleftarrow \phi + \Delta\phi(\phi)$$

All actuators except SECs have a fine telemetry potentiometer (fine TM pot) whose voltage ratio response at an actuator output shaft angle ϕ is given by

$$V = A + BG(\phi - \phi_n) + \Delta V_H(\phi) \pm \Delta V_D \qquad (5)$$

where A and B are regression coefficients, G is the gear ratio between the fine pot shaft and the actuator output shaft, ϕ_n is the effective central angle for the n^{th} revolution of the fine pot shaft, or

$$\phi_n = \phi_0 + \frac{n\ 360}{G}$$

and

$$n = \left\{ \frac{G(\phi - \phi_0)}{360} - \frac{1}{2} \right\}_{\text{truncated}}$$

and ΔV_H is a correction for harmonic errors that arise from gear axis offsets in the gear train between the fine pot shaft and the actuator output shaft,

$$\Delta V_H = \sum_{i=1}^{K} a_i \cos(g_i\ (\phi - \phi_0) + \delta_i) \qquad (6)$$

where a_i and δ_i are regression solutions for the amplitude and phase, respectively, and g_i is the gear ratio for the i^{th} gear in the train with respect to the actuator output shaft; K is the number of gears in the train, three for scan actuators and two for El actuators; ΔV_D is an average hysteresis correction, equal to half the difference between the forward and backward direction solutions for A.

C. DAC CALIBRATION

The DAC units were tested at GE Space Division, Valley Forge, Pennsylvania, and digital voltmeters were used to obtain all relevant voltages. The quantities measured were V_H and V_L, the high and low voltages across the DAC which provide the reference voltage, and the twenty DAC output voltages, V_j, which resulted from the twenty standard test commands, N_j. The test commands, in binary notation, are given in Table 3-1.

Table 3-1. Test Commands

Test command No.	Command bits	Command position
1	0 0 0 0 0 0 0 0 0 0	0
2	0 0 0 0 0 0 0 0 0 1	1
3	0 0 0 0 0 0 0 0 1 0	2
4	0 0 0 0 0 0 0 1 0 0	4
5	0 0 0 0 0 0 1 0 0 0	8
6	0 0 0 0 0 1 0 0 0 0	16
7	0 0 0 0 1 0 0 0 0 0	32
8	0 0 0 1 0 0 0 0 0 0	64
9	0 0 1 0 0 0 0 0 0 0	128
10	0 1 0 0 0 0 0 0 0 0	256
11	1 0 0 0 0 0 0 0 0 0	512
12	1 1 0 0 0 0 0 0 0 0	768
13	1 1 1 0 0 0 0 0 0 0	896
14	1 1 1 1 0 0 0 0 0 0	960
15	1 1 1 1 1 0 0 0 0 0	992
16	1 1 1 1 1 1 0 0 0 0	1008
17	1 1 1 1 1 1 1 0 0 0	1016
18	1 1 1 1 1 1 1 1 0 0	1020
19	1 1 1 1 1 1 1 1 1 0	1022
20	1 1 1 1 1 1 1 1 1 1	1023

One complete set of values of V_H, V_L, V_j, j = 1, 20, constituted one "test run," and a number of test runs were made for each channel of each DAC under varying conditions of temperature, other-channel interference, and variation of reference voltage. DAC Serial No. 003 had 24 test runs, and DAC Serial Nos. 004 and 005 had 18 test runs. The latter two DACs are the flight units, for which every third test run starting with the first was at ambient temperature, followed by high- and low-temperature runs. All data were processed, but ultimately only results from ambient runs were used in the mode, with interference, noninterference, and reference voltage effects being averaged.

The calibration data were processed as described below to obtain the regression coefficients for Eq. (2) in the form

$$VR_j = V_0 + \sum_{i=1}^{10} N_{ij}\,\Delta V_i$$

The noise correction, ΔV_N, has been set to zero by specifying all of its coefficients to be zero in the ARTC model data base. This was done because the noise effect was not found in the Spacecraft Assembly Facility test results and suffered from the lack of sufficiently complete experimental results for a full analysis. The noise that was observed during assembly-level testing is now considered to have been most probably a product of the test equipment. The ARTC model retains the logic for including electrical noise as a function of ARTC-E channel, slew rate, slew direction, and uncorrected voltage ratio, so that nonzero coefficients may be put into the data base at some future time if this is found to be necessary.

The following definitions will be used in the description of the DAC calibration:

V_H = positive voltage reference across the DAC

V_L = negative voltage reference across the DAC

V_j = voltage output from DAC for command N_j

N_j = command number for standard command No. j, where $1 \leq j \leq 20$

N_{ij} = i^{th} binary bit of command N_j, where $1 \leq i \leq 10$

VR_j = voltage ratio for $V_j = \dfrac{V_j - V_L}{V_H - V_L}$

W_{mn} = covariance matrix for the eleven quantities to be determined, V_0 and ΔV_i, where $1 \leq m, n \leq 11$

V_0 = residual voltage ratio, i.e., DAC output for $N_j = 0$

ΔV_i = voltage ratio increment for the i^{th} command bit
σ_0 = a priori measurement uncertainty, 2×10^{-5} voltage ratio

W_n^0 = values for the diagonal a priori covariance matrix W_{mn}; $W_n^0 = 10^{-2}$ was employed

P_n = estimate of the values of V_0, ΔV_i, where P_1 is the estimate of V_0, and P_n is the estimate of ΔV_{n-1} for $n > 1$

The first part of the calculation for one given set of values (V_H, V_L, V_j, $j = 1, 20$) is to put the V_j array in the same order as the standard N_j commands if the run was performed in the reverse order; then the VR_j array is calculated. Two different methods of estimation were employed, and each will be described separately. The first method is the sequential estimation method, and the second is a normal batch least squares calculation.

The sequential estimation method is described by the following sequence of operations:

(1) The covariance matrix is initialized to a priori estimates:

$$W_{mn} = 0, \quad m \neq n$$

$$W_{mn} = W_m^0$$

(2) Next, nominal values are inserted into P_n:

$$P_1 = V_0^{nom} = 2^{-11}$$

$$P_n = \Delta V_{n-1}^{nom} = 2^{n-12} \qquad 1 \leq n \leq 11$$

(3) Then the following computations are performed for each of the twenty measurements, where j is the measurement number:

$$u_K = \sum_i W_{iK} A_{ij}, \qquad K = 1, 11$$

where

$$A_{iK} = 1, \quad A_{n+1,K} = N_{nK}, \quad 1 \leq n \leq 10$$

$$b = \sigma_0^2 + \sum_k u_K A_{Kj}$$

$$c = \frac{1}{b}$$

$$Z_K = c\, u_K$$

$$d = \sum_K P_K A_{Kj}$$

$$\delta = VR_j - d$$

At this point a test is made to determine whether the data point No. j should be used in the estimation, i.e., whether an incorrect number was recorded, or the equipment suffered a transient. The value of δ is the deviation between the measured voltage ratio and the theoretical one for command N_j using current estimates for V_0 and ΔV_i. The test is:

IF ($c\delta^2$ > ACCEPT) write message and branch around this point

IF ($c\delta^2 \leq$ ACCEPT) use this point in the estimation

where ACCEPT is the square of the number of standard deviations from the current estimate within which a point is acceptable, and may be specified by the user. The value used was nine, or three standard deviations. If δ is too large, the next measurement is processed. If δ is acceptable, the calculation continues as follows:

$$P_K \leftarrow P_K + \delta Z_K, \qquad 1 \leq K \leq 11$$

$$W_{nK} \leftarrow W_{nK} - u_n Z_K, \qquad 1 \leq n, K \leq 11$$

(4) After all twenty measurements are processed, the P_K array contains the best estimates of V_0 and ΔV_i, and is printed out along with the accuracies, X_K, and the correlation matrix, Y_{jK}, where

$$X_K = \sqrt{W_{KK}}, \quad 1 \leq K \leq 11$$

$$Y_{jK} = W_{jK}/X_j X_K, \quad 1 \leq j, K \leq 11$$

(5) Then the twenty measurements are used with the final estimates P_K to calculate the final mean square fitting error:

$$\left.\begin{aligned} d_j &= \sum_K P_K A_{Kj} \\ \delta_j &= VR_j - d_j \end{aligned}\right\} \quad j = 1, \cdots, 2$$

$$\sigma^2 = \frac{1}{20} \sum_j \delta_j^2$$

A normal least squares approach was also implemented because of the tendency of a sequential estimation to become unstable under difficult circumstances. In practice, all DAC data was processed with both methods, and all results were identical. The "normal least squares" calculations were the following:

$$Z_{nK} = \sum_j A_{nj} A_{Kj} \qquad j = 1, \cdots, 20$$

$$u_K = \sum_j A_{Kj} VR_j$$

where A is defined as in the sequential method

$$P_K = (Z_{nK})^{-1} u_K$$

This gives the estimates for V_0 and ΔV_i in the vector P_K, which is printed out along with the quantities $\bar{\delta}_j$ and σ defined in the sequential method.

The twenty measurements that employ the twenty standard commands, N_j, were repeated for varying combinations of temperature and interference. For the flight units, this produced a total of eighteen runs each. Typical fit accuracy for these runs was ± 0.00005 in VR. The results for P_K were stored for all eighteen runs, and then the mean solutions for each P_K, namely $\bar{P}_K$, were calculated by averaging over all runs. This averaging was then repeated with only the results from the ambient temperature runs. Standard deviations were computed in both cases for each $\bar{P}_K$ and were typically 0.00001 in VR. Essentially, all variation from run to run was contained in V_0 and was typically ± 0.00015. The ambient temperature averages and standard deviations were not appreciably different from those using all eighteen runs, but the ambient temperature results were inserted into the data base.

One of the hardware tests performed at SAF is essentially a low-resolution version of the actuator integration test performed in the laboratory. The actuator is slewed from some low command position to some high one, and then back to the low one; in the process, command positions 128, 256, 384, 512, 640, 768, and 896 are used, and telemetry voltages and DN are recorded at each position. The ARTC-E channel used in the slew is flip-flopped for each slew. Comparison of the SAF results with the ARTC model indicated that a slight bias and slope error existed in the DAC model. This was attributed to small variations in the gain of a buffer amplifier, which were neither monitored nor recorded in the DAC calibration runs. Corrections to the effective bias and slope were made for each channel of each DAC.

D. ACTUATOR CALIBRATION

The actuator assembly-level testing was performed in the laboratory at JPL. For each actuator test run, the actuator was slewed without a load to its low end (FB pot voltage near zero), and voltages monitored by a digital voltmeter were recorded on magnetic tape for several hundred "invariant" measurements, along with the output of a shaft angle encoder. Voltages were recorded from each pot (FM-A, FM-B, coarse TM, fine TM). After the invariant data were recorded, the actuator was slewed forward, with one set of measurements (V_{FBA}, V_{FBB}, V_C, V_F, ϕ) taken at every fifth motor pulse. When the high angle limit was reached, the actuator was slewed in the backward direction with measurements continuing to be recorded until the low end was reached, after which several hundred more "invariant" measurements were made. At this point the tape drive put an end of file mark on the tape. Each actuator was processed at least twice as described, once after thermal-vacuum testing, and once after completion of testing. Some actuators were processed numerous times under various conditions to determine the best lab setup, e.g., with and without a brake, with encoder coupling loose and tight. The best data were found to result from a tight coupler with no brake. The best two test runs for each actuator were used in the calibration analysis, with the final data for the ARTC model data base taken from only one of these runs.

The data employed were put into voltage ratio form by normalizing to the reference voltage. Sequential estimation programs were employed to obtain the regression coefficients for the FB and coarse TM pot linear models, and hysteresis and nonlinearity effects. The hysteresis corrections were set equal to half the forward-backward angular difference, with the mean angle as nominal. Domains for the piecewise-linear corrections were generated by hand from the hysteresis plots which the programs provided. The FB pot nonlinearity corrections for each channel were obtained by hand smoothing the separate results for each slew direction.

The fine TM pots were calibrated by both sequential and batch regression, like the DAC. The results of the batch regression had lower fitting errors because of that method's lesser sensitivity to delicate terms such as the gear harmonics.

The result of fitting a fine pot to the linear plus harmonic terms is generally that all the regression coefficients come out the same for both slew directions except the constant term A. This is to be expected, because this is the influence that gear train hysteresis would have, and we expect to find some hysteresis of this sort. Thus, if A_f and A_b are the forward and backward direction solutions for A, respectively, then

$$A = \frac{1}{2}(A_f + A_b)$$

$$\Delta V_D = \frac{1}{2}(A_b - A_f)$$

Then the model uses $A - \Delta V_D$ for the forward direction, and $A + \Delta V_D$ for the backward.

The harmonic amplitude and phase parameters of Eq. (6) cannot be determined directly by normal linear regression techniques since they violate the basic assumption of linearity over the range of uncertainty. However, the parameters of the harmonic error can be determined if the equation is rewritten as:

$$\Delta V_H(\phi) = \sum_{i=1}^{N} \{a'_i \sin g_i\theta + b'_i \cos g_i\theta\}$$

where $\theta = \phi - \phi_0$, g_i is the i^{th} gear ratio in the fine pot gear train, $N = 4$ for scan actuators, and $N = 3$ for elevation actuators. Note that an extra frequency, the fundamental, is included here, whereas it is not included in the model; this is because the fundamental harmonic results from misalignments of the actuator output shaft with the encoder shaft, and does not apply to the alignment of the actuator output shaft with its load. Thus this term absorbs the fundamental harmonic, allowing the others to be estimated better. The actual alignment error for the shaft and load must be evaluated by in-flight calibration, and the correction is made exterior to the ARTC model.

The regression solution yields a'_i, b'_i, $i = 1, 2, \cdots K$. Then these values are used to obtain the values of a_i and δ_i of Eq. (6).

$$\left.\begin{aligned} a_i &= \sqrt{(a'^2_{i+1} + b'^2_{i+1})} \\ \delta_i &= \tan^{-1}(-a'_{i+1}/b'_{i+1}) \end{aligned}\right\} \quad 1 \leq i \leq K$$

During the assembly-level calibrations, it became apparent that the angular alignments of the actuator output shafts with the encoder shaft were subject to errors great enough to merit attention. The assumption that the actuator shaft central position would be aligned sufficiently accurately with the encoder 180-deg position was abandoned, and the actual encoder position was written on the tape reel label. The central angle thus supplied was used in the analysis programs where the default value of 180 deg would otherwise have been used. It was discovered later that the central angles reported for some actuators were inconsistent from one run to another of the same actuator, because angular shifts with respect to the responses of the four pots were detected. The relative tracking of the pots with respect to each other was extremely reproducible from run to run, so the reported central angles were assumed to have been unreliable.

The only significant error introduced by erroneous central angle values is in the constant term A of the model linear equation for the pots. Note that these equations really contain two constant terms,

A and $-B\phi_0$ (the latter is $-BG\phi_n$ for fine pots). Thus a systematic error in ϕ_0 produces an additive error in A. Second-order errors are all negligible. This ambiguity in ϕ_0 was the reason why one-run results were used to load the ARTC model data base rather than some suitable average of two or more runs. This simplified the handling of the fine pot harmonics, and left only the central angle in doubt for each actuator.

The following data were used to adjust the scan platform and antenna actuator central angles in the ARTC model data base: angle position, ϕ_c, measured with the assembled scan platform or antenna in the latched position; coarse pot voltage ratio, VR_c; and fine pot voltage ratio, VR_f. The single-point calibration correction procedure performed the following sequence of operations:

(1) Convert VR_c and VR_f to floating point data number, DN_c and DN_f.

(2) Pass DN_c and DN_f to the ARTC model for telemetry processing; the ARTC model returns the achievable angle which corresponds to DN_c and DN_f according to the ARTC model data base, ϕ_m;

(3) Calculate

$$\Delta\phi = \phi_m - \phi_c$$

$$\phi_0^i \longleftarrow \phi_0^i - \Delta\phi, \quad i = 1, 2, 3, 4$$

where ϕ_0^i is the central angle (corrected) for the i^{th} pot (feedback-A, feedback-B, coarse, and fine).

(4) $\Delta\phi$ and the ϕ_0^i are written on the printer.

The new ϕ_0^i values were then put into the ARTC model data base, after which check runs were made to insure that the program produced $\Delta\phi = 0$.

Some idea of the modelling accuracy achieved may be obtained from typical calibration residuals representing deviations corresponding to a 95% confidence level. For the feedback pots, this is ± 0.07 deg on the output shaft (including a lookup table to correct for unmodelled nonlinearities); for the coarse telemetry pots it is ± 0.25 deg, and for the fine telemetry pots, ± 0.02 deg.

SECTION IV

IN-FLIGHT CALIBRATION

A. INTRODUCTION

This section and the next summarize the results of processing over five-hundred Viking Orbiter pictures used either for the purpose of in-flight calibration of the scan platform and camera (VIS) alignment, or for the approach optical navigation sequences. New software and processing techniques were developed to meet the demanding processing schedules and large volume of pictures required by the Viking mission. An integrated approach was applied to all of the scan platform calibration sequences. Not only did they serve to calibrate the scan platform alignment and VIS response, but they were designed to assist in developing and refining processing techniques to be employed for the approach optical navigation sequences. The merits of this integrated approach were clearly demonstrated by the approach optical navigation sequences where, for the first time, the optical data were used as a principal navigation data type for an interplanetary mission. The optical based orbit determination was, in fact, the primary cause of the exceptional interplanetary navigation accuracy experienced by both Viking Missions. In addition to the successful approach navigation, the following accomplishments resulted from the scan platform calibration and early instrument check out picture sequences:

(1) First maneuvered picture for a JPL spacecraft (Earth departure pictures).

(2) Greatest distance of an Earth photograph.

(3) Development of both a new control and knowledge-type scan platform hysteresis model.

(4) New camera distortion model and automated calibration.

(5) Advances in accurate and rapid optical measurement processing and picture planning.

B. OPTICAL MEASUREMENT SOFTWARE SET (OMSET)

The following programs were used in flight operations on the UNIVAC 1108 to plan and process picture sequence data for the scan platform calibration and approach optical navigation picture sequences:

(1) Probability of Stars Evaluation (POSE): A fast-running program used to determine optimum scan platform pointing in terms of probable data return. This program was designed specifically for the approach Mars pictures, but was also used for scan calibration pictures.

(2) Automatic Video Flyback Telemetry Extraction (AUTOFLY): A program that extracts from a VIS EDR tape the engineering telemetry imbedded in the picture flyback data when the picture was recorded.

(3) Translation of Stars (TRANS): This program takes a file that contains the predicted star locations based on engineering telemetry and automatically creates an input file for the IMP program, specifying the picture areas to be extracted.

(4) Reseau Extraction and Calibration (RESCAL): Using the raw picture tape (VIS EDR) as input, the program/run-stream automatically extracts and locates reseau images, and does a camera distortion model calibration. The complete calibration process takes less than ten minutes total throughput time per picture.

(5) Celestial Geometry Generator (CGG): A MM'71 program modified for Viking application that simulates celestial geometry of stars and planets within a given picture or picture pair.

(6) Image Processing (IMP): A MM'71 program modified for Viking application that accesses the VIS EDR to printout selected areas within a given picture. This program also does the Mars image center estimation process.

(7) Optical Data Calibration and Rectification (ODCR): A MM'71 program expanded and modified for Viking application. This program performs the conversion of and estimation process on the telemetry and image location data, and provides estimated model parameters for input to the Scan Platform Operations (SCANOPS) Program and a processed optical navigation observables for the Optical Navigation Program (ONP).

C. IN-FLIGHT SCAN PLATFORM CALIBRATION SEQUENCE OBJECTIVES

The in-flight calibration of the attitude control (Sun and star) sensors, scan platform alignment, and VIS alignment is necessary to point the scan platform-mounted science instruments, including the VIS, and to determine their pointing directions from downlink telemetry to the accuracy required for the science experiments and optical navigation. The accuracy with which the scan platform must be positioned (pointing control) is 0.5 deg (99%), and the accuracy with which the scan platform position must be determined (pointing knowledge) is 0.25 deg (99%). These requirements apply when the spacecraft is on celestial references.

For each Viking Orbiter, five distinct picture sequences were planned to calibrate the scan platform: Instrument Check-Out and Scan Cal I through IV. The primary objectives for each of these sequences were:

(1) Instrument Check-Out: This sequence was designed primarily to provide early information on the totally new technique of a two-camera operation for optical navigation using the Earth in one camera and stars in the adjacent camera. In addition, this sequence provided early indications of camera response characteristics and a limited scan platform calibration.

(2) Scan Cal I: Initially this sequence was intended to remove any large scan platform offsets before going into a complete calibration sequence. However, based on the good results of the instrument check-out sequence this sequence was changed into a complete scan platform calibration sequence.

(3) Scan Cal II: Primary objective was to verify the results of Scan Cal I, and to photograph Mars and determine critical approach optical navigation processing procedures.

(4) Scan Cal III: Intended to verify scan platform pointing control and knowledge after Mars orbit insertion and before lander separation.

(5) Scan Cal IV: Complete calibration sequence to develop model parameters that apply to the entire region available to the scan platform after the lander has been separated.

D. INSTRUMENT CHECK-OUT SEQUENCE

The instrument check-out sequence consisted of an initial picture pair of stars, followed seven days later by two picture pairs with the Earth in one camera and stars in the other camera. At the time selected for the pictures, this was possible only with a spacecraft roll maneuver. The purpose of the star pair scheduled seven days prior to the Earth pictures was to obtain added confidence that the spacecraft hardware was working properly, and that the VIS cameras and the science instrument platform pointing was understood. This precaution was taken since any one of a number of malfunctions or misunderstandings could cause gross overexposure of the vidicons when taking the Earth-star pair.

1. Picture Sequence Design

The following constraints were applied in selecting star targets for the initial Viking Orbiter pictures:

(1) Scan platform clock and cone gimbal angles should be near the angles required for Earth-star pictures to verify pointing in this region, and to maintain a similar slewing sequence (rate and direction) to minimize any hysteresis effects.

(2) For a pointing control error of 1 deg (0.59 deg is predicted), select a star field that will result in a high probability of having at least one star brighter than a visual magnitude of seven in each camera.

(3) Pointing should be greater than 1.5 deg from the Earth or Moon direction at the time of the star picture to insure against overexposing the vidicon.

To satisfy the above constraints, the Probability of Stars Evaluation (POSE) Program was used. This program was developed for the Viking mission to provide an analytic and efficient evaluation criteria for designing picture sequences for scan calibration and optical navigation. The use of the POSE program will be discussed further in the section on the determination of the pointing directions for the optical navigation pictures.

The nominal inertial pointing direction selected by POSE for the scan platform based on the above constraints for both Viking Orbiter 1 (VO-1) and Viking Orbiter 2 (VO-2) was right ascension 270.985 deg and declination -3.83 deg. Table 4-1 gives the results of this pointing.

Seven days after the initial star pair picture, two picture pairs were to be taken where, for each pair, the Earth was in one camera (short exposure) and stars in the other camera (long exposure). The primary objectives of this sequence were to:

(1) Provide a data type similar to optical navigation control picture sequences for ground software processing verification (first time this particular technique was used for optical measurement processing).

Table 4-1. Probability Distributions for Stars

Viking Imaging System	Probability of at Least One Star (Brighter Than Visual the Magnitude Below) Being in Designated Camera for a 1.0- and 0.59-deg Pointing Control Error					Pointing Control Error, deg
	Star Visual Magnitude Less Than					
	4	5	6	7	8	
A	0.0	0.06	0.63	0.97	1.0	1.00
	0.0	0.	0.95	0.98	1.0	0.59
B	0.0	0.11	0.21	0.99	1.0	1.00
	0.0	0.	0.0	1.0	1.0	0.59

(2) Verify uplink and downlink processing prior to scan calibration sequence.

(3) Test and provide VIS sensitivity levels to stars and planets.

(4) Verify camera focus and responsivity.

(5) Provide vidicon raster shift measurement for geometric distortion removal.

(6) Determine light flood pedestal level.

A constraint on the Earth picture was to bias the nominal position of the Earth to insure keeping the Earth out of the overlap region of the VIS field of view. Considering the nominal time of the pictures (Day 293, VO-1 and Day 289, VO-2), the Earth's position in its VIS frame could be designed 0.59 deg (99% uncalibrated control error prediction) inside the outer edge of the field of view and 0.76 deg from the overlap region. The time of this picture pair was constrained by the Earth-star-Moon background geometry that resulted from the actual trajectory. Figures 4-1 and 4-2 illustrate the cone/clock angle directions for the Earth. These figures show that the Earth is nominally outside the scan platform's field of view so that it was necessary to perform a roll maneuver prior to taking the Earth pictures.

2. Unexpected Events

Two events occurred that were not anticipated:

(1) In both the star and Earth-star picture pairs considerable glare was visible in the long exposure star frame; this phenomenon, called "veiling glare," was a subject of discussion until the Scan Cal I pictures. Some theories proposed that the glare was the result of the Earth's reflection into the star camera and, if this was the case, problems may have resulted in the optical navigation sequences. The amount of glare in these pictures seemed to correlate well with decreasing cone angle rather than the Earth's position with respect to a given frame. This fact hinted at the possibility that it was either direct or reflected sunlight.

(2) On VO-1, the Earth was missed in one of the picture pairs due to an oversight in validating sequences; as a result of this occurrence, procedures were refined to prevent any future problem of this nature.

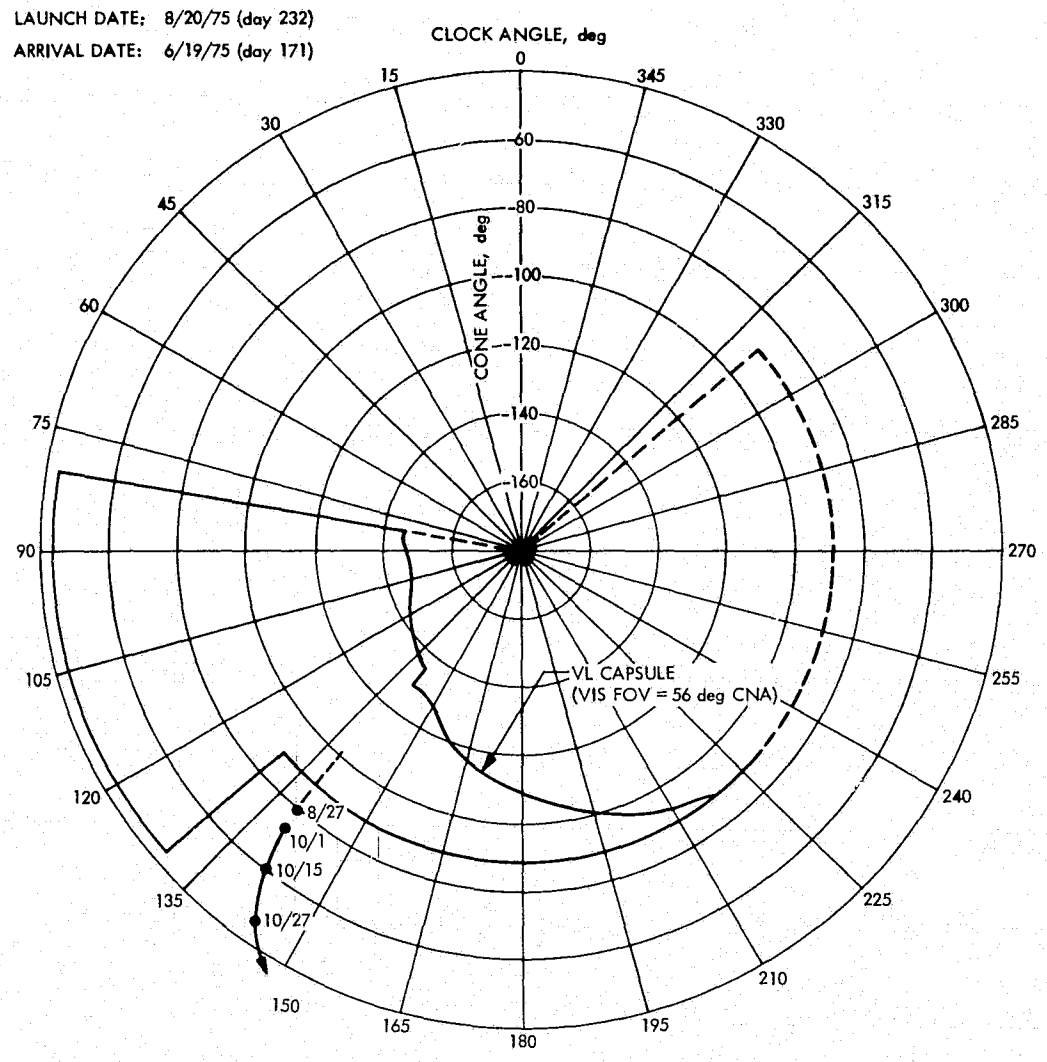

Figure 4-1. Track of Earth in Celestial Cone and Clock, VO-1

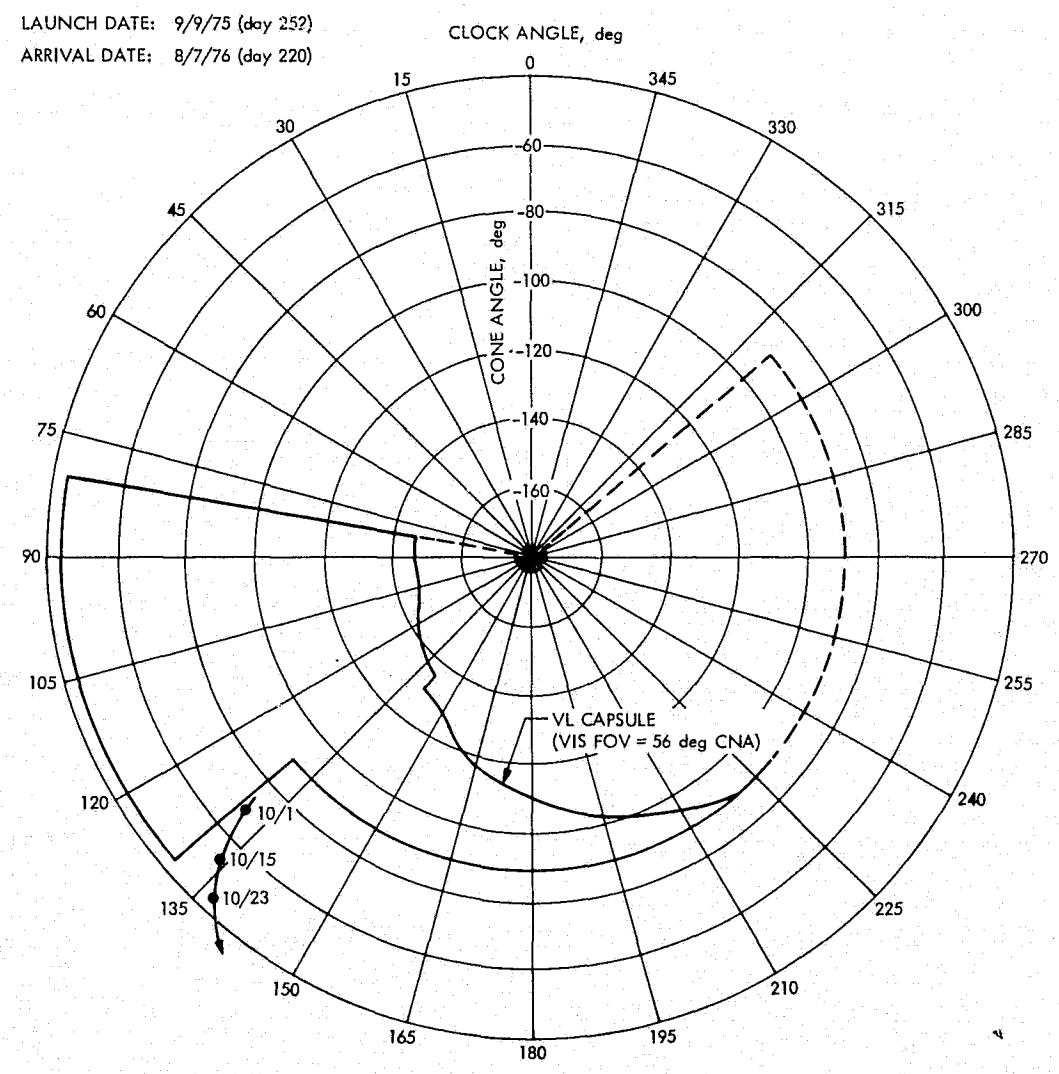

Figure 4-2. Track of Earth in Celestial Cone and Clock, VO-2

3. Summary of Analytical Results

a. Picture Pointing.[1] The following procedure was used in estimating offsets involved in picture pointing using the star-pair-picture data and engineering telemetry as input to OMSET:

(1) Using ground determined VIS distortion and camera offsets, solve for three scan platform offsets:

$\Delta\alpha$ = scan platform clock offset
$\Delta\beta$ = scan platform cone offset
$\Delta\omega$ = scan platform rotation offset

Table 4-2 contains the estimated values, and it was these offsets that were the basis upon which changes to the Earth-star picture sequences were made.

(2) Using the above estimated offsets, ground VIS offsets, and a flight calibrated VIS distortion model parameters, solve for the following parameter set:

$\Delta\alpha$ = scan platform clock offset
$\Delta\beta$ = scan platform clock offset
$\Delta\omega$ = scan platform rotation offset
ψ_A = VIS A cone offset
X_A = VIS A cross-cone offset
ω_A = VIS A rotation offset
ω_B = VIS B rotation offset

Table 4-3 has the estimated values for the above set of parameters.

Table 4-2. Estimated Scan Platform Offsets

Parameter	Offset, deg	
	VO-1	VO-2
$\Delta\alpha$	-0.329	+0.234
$\Delta\beta$	+0.169	+0.172
$\Delta\omega$	+0.064	-0.120

[1] Individual pictures are referenced by picture number, e.g., 293C04 is the fourth picture taken on day 293 by VO-1(C).

Table 4-3. Camera and Scan Platform Offsets

Parameter	Offset, deg	
	VO-1	VO-2
$\Delta\alpha$	-0.322	+0.231
$\Delta\beta$	+0.170	+0.174
$\Delta\omega$	+0.044	-0.087
ψ_A	-0.008	-0.023
X_A	-0.709	-0.679
ω_A	-0.290	-0.337
ω_B	-0.001	-0.340

(3) Using the parameters calibrated in (2) and the calculated limit cycle rates, process the Earth-star pictures and solve for a common clock, cone, pitch, yaw, and roll offset for each pair to determine camera pointing. Table 4-4 summarizes the camera pointing that resulted from (2) for the star pairs, and from (3) for the Earth-star pairs. The "desired pointing" corresponds to the mission planning level pointing; "engineering telemetry pointing" corresponds to the pointing as reconstructed from the celestial sensor position telemetry, rate estimates, gyro limit-cycle position and drift estimate, roll-turn rate estimate, and the scan platform gimbal angle telemetry; "estimated pointing" is the result of using star images to determine camera pointing. Table 4-5 summarizes pointing control (desired minus estimated) and knowledge (engineering telemetry minus estimated).

b. Earth Image Center Finding (VO-2). Even though the Earth image saturated the telemetry (data number (DN) = 127), the image was of good quality for center finding; i.e., the usual nemesis of planets and satellites in the same frame with stars are not of major concern (blooming, smearing, spreading, beam bending). Prior to processing the Earth image, it was decided to determine limb points at a level approximately 50% between the background and the peak signal for the Earth image. This decision was based on the analysis of ground star planet pictures taken for optical measurement studies, and the fact that, for any purely symmetric vidicon point spread function convolved with a step function (limb), the 50% point corresponds to the limb.

Table 4-4. Camera Pointing Summary and Instrument Check-Out

Picture ID	Desired			Engineering Telemetry			Estimated			No. of Stars Used
	Clock	Cone	Twist	Clock	Cone	Twist	Clock	Cone	Twist	
VO-2										
282D01	123.45	73.26	0.21	123.56	72.97	-0.24	123.80	73.14	-0.44	7
282D02	124.89	73.26	-0.21	124.97	72.95	-0.85	125.20	73.13	-0.85	3
289D01	134.72	52.38	0.53	134.75	52.42	-0.11	134.73	52.36	-0.10	—
289D02	136.46	52.38	-0.53	136.44	52.41	-1.14	136.42	52.35	-1.1	4
289D03	132.46	52.38	0.53	132.62	52.51	0.05	132.59	52.48	0.06	2
289D04	134.20	52.38	-0.53	134.40	52.49	-0.98	134.28	52.46	-0.97	—
VO-1										
286C01	123.07	66.53	0.30	123.17	66.69	-0.04	122.84	66.86	0.06	6
286C02	124.57	66.53	-0.30	124.67	66.66	-0.22	124.35	66.83	-0.25	5
293C01	141.71	55.73	0.47	141.38	55.65	0.08	141.42	55.63	0.07	—
293C02	143.37	55.73	-0.47	143.05	55.64	-0.57	143.10	55.62	-0.59	5
293C03	139.43	55.73	0.47	138.69	55.42	0.34	138.66	55.48	0.34	5
293C04	141.09	55.73	-0.47	140.37	55.39	-0.33	146.34	55.45	-0.32	—

Table 4-5. Pointing Control and Knowledge

Picture ID	Control Error, deg			Knowledge Error, deg		
	$\Delta\alpha$	$\Delta\beta$	$\Delta\omega$	$\Delta\alpha$	$\Delta\beta$	$\Delta\omega$
VO-2 282D01	-0.35	+0.12	+0.65	-0.24	-0.17	0.20
282D02	-0.31	+0.13	+0.64	-0.23	-0.18	0
289D01	-0.01	+0.02	+0.59	+0.02	+0.06	-0.05
289D02	+0.04	+0.03	+0.57	+0.02	+0.06	-0.04
289D03	-0.13	-0.10	+0.43	+0.03	+0.03	-0.05
289D04	-0.08	-0.08	+0.41	+0.02	+0.03	-0.04
VO-1 286C01	+0.23	-0.33	+0.25	+0.33	-0.17	-0.09
286C02	+0.22	-0.30	-0.11	+0.32	-0.17	-0.03
293C01	+0.29	+0.10	+0.40	-0.04	+0.02	+0.01
293C02	+0.27	+0.11	+0.06	-0.05	+0.02	+0.02
293C03	+0.77[a]	+0.25	+0.13	+0.03	-0.06	0.00
293C04	+0.75[a]	+0.28	-0.29	+0.03	-0.06	-0.201

[a]0.3 deg due to a command error.

The following is a description of the limb determination process for the Earth:

(1) Search the raw video data from the bottom of the picture up in the increasing pixel direction and find two lines in a row with a signal level greater than a DN of eighty for 289D01/2 and ninety DN for 293C01 (threshold level).

(2) Using the first value greater than the threshold value (largest line number for a fixed pixel number) interpolate to find the line position where the threshold level occurs.

Once the limb points are determined by the above algorithm, an ellipse corresponding to the Earth's eccentricity and orientation in camera coordinates was to fit to the limb points; the results are given in Table 4-6.

Table 4-6. Results of Limb-Fitting Process

Parameter	Picture ID		
	289D01	289D04	293C01
Line No. of Center	424.15	501.10	412.30
Pixel No. of Center	482.44	727.88	596.68
Image Semimajor Axis, pixels	22.4	22.2	13.9
Mean of Fit, pixels	0.02	0.05	0.09
Standard Deviation in Radius, pixels	0.07	0.11	0.12
Number of Limb Points Fit	43.0	43.0	24.0

c. Earth Residuals (VO-2). Using the image centers resulting from the previously described image center finding process and the camera pointing in Table 4-4, the following Earth residuals resulted (observed minus expected):

Picture	Line	Pixel
289D01	1.48	0.81
289D04	-0.39	-1.36
293C01	-1.65	-0.45

The following error sources are included in these residuals:

(1) Camera-to-camera alignment.

(2) Camera distortion.

(3) Earth center finding.

(4) Star image location uncertainties as mapped to camera pointing.

(5) Limit-cycle rates between pictures (Table 4-7).

(6) Trajectory.

The magnitude of the Earth residuals are of a level that corresponded to satisfactory processing predictions (<2 pixels) and were very important data points in establishing that the optical navigation control picture sequences (stars-Mars-stars) would result in a good observable for navigation. Subsequent analysis resulting from scan platform calibration pictures (more accurate camera-to-camera alignment, stars-Mars-stars triad processing, veiling glare experiments, etc.) augmented these early pictures with information to establish the merits and problems associated with processing the Mars image for a navigation observable.

d. Camera Distortion. As a result of analysis of ground calibration pictures a new distortion model was developed that incorporated distortion correlations between lines and pixels. As a result of this distortion model, residual distortion errors were reduced by a factor of three (0.75 pixel to 0.25 pixel). Table 4-8 contains the in-flight distortion calibration accuracy results.

E. SCAN PLATFORM CALIBRATION SEQUENCE I

1. Picture Sequence Design

During the cruise phase, the first orbiter scan platform calibration sequences were scheduled on day 40 (February 9, 1976) for VO-1 and

Table 4-7. Limit-Cycle Rates Mapped to Camera Coordinates

Picture ID	Image Rates	
	Lines/s	Pixels/s
282D01/2	0.4	0.4
286C01/2	-0.1	-0.1
289D01/2	0.6	0.6
289D03/4	0.2	0.6
293C01/2	1.3	0.1
293C03/4	0.0	0.2

Table 4-8. Distortion Calibration Results, Reseau Statistics, 1 σ

Coordinate	VO-1		VO-2	
	A-Camera	B-Camera	A-Camera	B-Camera
	S/N 7	S/N 4	S/N 8	S/N 6
Line	0.25	0.27	0.22	0.27
Pixel	0.34	0.26	0.19	0.25

day 434 (February 13, 1976) for VO-2 to remove any large offsets in the platform pointing. These sequences originally consisted of six five-picture strips and one three-picture swath of stars. The strips provided a mosaic of pictures large enough to guarantee seeing the stars with large pointing control errors. However, based upon the results of processing the Earth and star pictures taken during the instrument checkout sequences conducted in October 1975, it had been determined that offsets were characterized well enough that Scan Cal I could be used to provide a more comprehensive scan platform calibration and meet many of the objectives originally intended for Scan Cal II. Scan Cal II could then be used for verification of the Scan Cal I results and used for optical measurement processing studies in preparation for the important optical navigation sequences.

Scan Cal I consisted of nineteen one-picture swaths, six two-picture swaths, and two three-picture swaths for a total of 37 pictures. The following considerations were designed into the picture sequences:

(1) Comprehensive coverage of scan platform pointings and VIS field-of-view available with the lander attached.

(2) Picture pairs taken at the identical scan platform pointing (spacecraft referenced) as that used for the star and Earth-star picture pairs during the instrument checkout sequences (paths). These pictures were used to determine if the "veiling glare" characteristics that occurred during the instrument checkout sequence was Sun or Earth induced.

(3) Approximate Mars approach clock and cone pointing and hysteresis check of this region.

(4) Picture pair pointed at the star field intended for control optical navigation.

(5) Two triads of the Pleiades for camera-to-camera alignment determination.

(6) Addition of a final two-picture swath in the sequence to maintain a time history of camera distortion as a function of the exposures anticipated for the Mars approach pictures.

(7) Nearly even distribution of positive and negative cone and clock slews for hysteresis analysis.

(8) Check to insure that no planets are near the VIS field-of-view (overexposure).

(9) Keep the number of pictures close to the original budget (37 versus 33).

(10) Choose identical star fields for VO-1 and VO-2 where possible (sensitivity analysis).

(11) Have the pictures taken during the normal working hours.

(12) The Earth's moon will not interfere with spacecraft telemetry.

(13) Pictures at short exposures typical for Mars navigation pictures for distortion analysis.

The Orbiter scan platform calibration sequence consisted of 27 VIS swath events during which time a total of 37 VIS pictures were recorded. Tables 4-9 and 4-10 present the VIS swath events numbered from 1 through 27 for VO-1 and VO-2, respectively. Other parameters shown on these tables associated with these 27 events are the Picture Number (040C01 for VO-1, 044D01 for VO-2, etc.), the time (GMT) of shuttering of the first VIS frame, number of pictures recorded, spacecraft scan platform pointing in clock (CLA) and cone (CNA) angles, and the brightest star that is expected to be within the recorded pictures. The scan platform pointing given in these tables is graphically illustrated in Figure 4-3. The picture pairs for both spacecraft during the VIS swath events Nos. 10 and 11 were targeted to duplicate the pointing of the star/star and Earth/star pictures taken during the October, 1975, instrument checkout sequences to evaluate the veiling glare problem.

2. Unexpected Results

The following events occurred during the Scan Cal I sequence that can be considered nonstandard:

(1) No recognizable star pattern was identified for picture 44D04 for VO-2, thus the scan platform pointing could not be determined. Subsequent sequences (extended region calibration) indicated that nothing peculiar in the scan platform behavior existed in this region, a possible conclusion might be that the VIS field-of-view may have been obstructed by the lander.

(2) After careful analysis of both the scan platform pointing based on stars and the predicted and actual gimbal angle

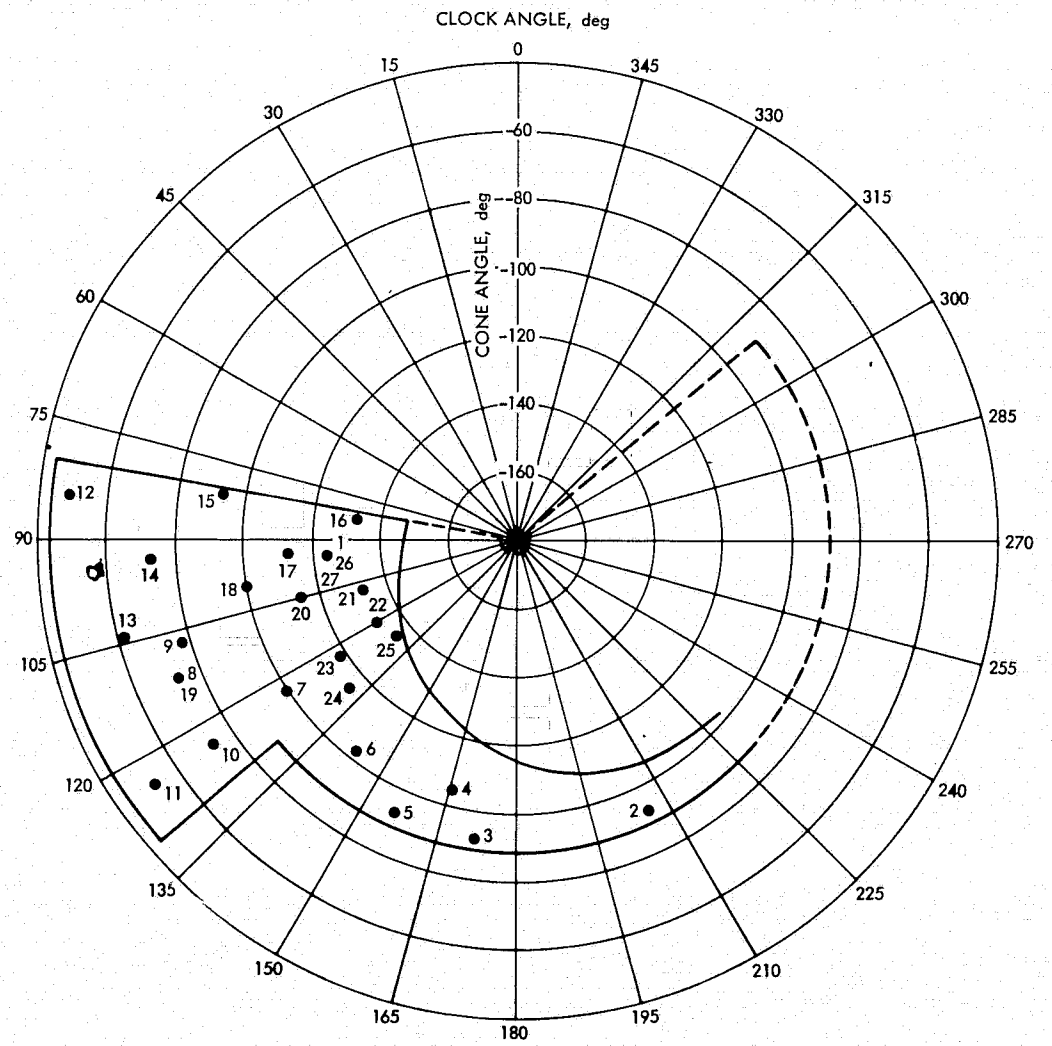

Figure 4-3. VO-2 Scan Cal I Instrument Pointing History

Table 4-9. VO-1 Scan Cal I Picture Sequence

Event No.	Picture No.	Time (OET-2/9/76)	Event	Scan Platform Pointing		Brightest Star (Visual Magnitude)	Notes
				Clock	Cone		
1	040C01/2/3	16:30:00	3-picture swath	95.40	127.70	3.0	Pleiades
2	040C04	16:50:00	1-picture swath	207.18	91.76	5.7	
3	040C05	17:00:00	1-picture swath	173.13	93.51	5.4	
4	040C06	17:10:00	1-picture swath	167.35	106.31	5.4	
5	040C07	17:20:00	1-picture swath	156.82	94.76	5.7	
6	040C08	17:30:00	1-picture swath	143.82	105.01	5.5	
7	040C09	17:40:00	1-picture swath	124.30	101.77	5.0	
8	040C10/11	17:50:00	2-picture swath	119.00	95.05	3.9	≈α, β Mars approach
9	040C12	18:00:00	1-picture swath	107.68	80.40	6.0	
10	040C13/14	18:10:00	1-picture swath	123.50	66.70	4.9	Star pair α, β
11	040C15/16	18:20:00	2-picture swath	123.50	55.64	5.7	Earth-star α, β
12	040C17	18:30:00	1-picture swath	85.02	52.70	5.6	
13	040C18	18:40:00	1-picture swath	104.32	64.85	5.3	
14	040C19	18:50:00	1-picture swath	93.94	75.94	5.6	
15	040C20	19:00:00	1-picture swath	81.23	95.95	4.8	
16	040C21	19:10:00	1-picture swath	83.49	136.10	3.6	
17	040C22	19:20:00	1-picture swath	94.95	116.31	4.6	
18	040C23	19:30:00	1-picture swath	100.68	103.04	4.8	
19	040C24/25	19:40:00	2-picture swath	119.00	95.05	3.9	≈α, β Mars approach
20	040C26	19:50:00	1-picture swath	106.76	117.52	5.2	
21	040C27	20:00:00	1-picture swath	109.88	135.74	5.6	
22	040C28	20:10:00	1-picture swath	122.89	135.47	6.1	

Table 4-9. VO-1 Scan Cal I Picture Sequence (Continuation 1)

Event No.	Picture No.	Time (OET-2/9/76)	Event	Scan Platform Pointing		Brightest Star (Visual Magnitude)	Notes
				Clock	Cone		
23	040C29	20:20:00	1-picture swath	125.36	120.77	6.0	
24	040C30	20:30:00	1-picture swath	133.72	116.58	4.0	
25	040C31/32	20:40:00	2-picture swath	150.31	129.59	6.7	Control star field
26	040C33/34/35	20:50:00	3-picture swath	95.40	127.70	3.0	Pleiades
27	040C36/37	20:55:00	2-picture swath	95.40	127.70	—[a]	

[a]Camera control word VIS-A 084LG (Exposure = 25 ms).
Camera control word VIS-B 104LG (Exposure = 51 ms).

Table 4-10. VO-2 Scan Cal I Picture Sequence

Event No.	Picture No.	Time (OET-2/9/76)	Event	Scan Platform Pointing		Brightest Star (Visual Magnitude)	Notes
				Clock	Cone		
1	044D01/2/3	16:30:00	3-picture swath	94.00	124.65	3.0	Pleiades
2	044D04	16:50:00	1-picture swath	206.13	93.53	5.7	
3	044D05	17:00:00	1-picture swath	172.01	93.50	5.4	
4	044D06	17:10:00	1-picture swath	165.52	105.78	5.4	
5	040D07	17:20:00	1-picture swath	155.67	93.86	5.7	
6	044D08	17:30:00	1-picture swath	142.20	103.44	5.5	
7	044D09	17:40:00	1-picture swath	122.99	99.38	5.0	
8	044D10/11	17:50:00	2-picture swath	112.16	73.73	7.0	≈α, β Mars approach
9	044D12	18:00:00	1-picture swath	107.02	77.52	6.0	
10	044D13/14	18:10:00	2-picture swath	124.30	73.32	7.0	Star pair α, β
11	044D15/16	18:20:00	2-picture swath	124.05	52.55	6.1	Earth-star α, β
12	044D17	18:30:00	1-picture swath	84.21	49.53	5.6	
13	044D18	18:40:00	1-picture swath	103.99	61.90	5.3	
14	044D19	18:50:00	1-picture swath	93.19	72.83	5.6	
15	044D20	19:00:00	1-picture swath	80.31	92.78	4.8	
16	044D21	19:10:00	1-picture swath	82.51	132.93	3.6	
17	044D22	19:20:00	1-picture swath	93.71	113.21	4.6	
18	044D23	19:30:00	1-picture swath	99.56	100.02	4.8	
19	044D24/25	19:40:00	2-picture swath	112.16	73.73	7.0	≈α, β Mars approach
20	044D26	19:50:00	1-picture swath	105.21	114.60	5.2	
21	044D27	20:00:00	1-picture swath	107.57	132.89	5.6	
22	044D28	20:10:00	1-picture swath	120.00	132.98	6.1	

Table 4-10. VO-2 Scan Cal I Picture Sequence (Continuation 1)

Event No.	Picture No.	Time (OET-2/9/76)	Event	Scan Platform Pointing		Brightest Star (Visual Magnitude)	Notes
				Clock	Cone		
23	044D29	20:20:00	1-picture swath	123.23	118.39	6.0	
24	044D30	20:30:00	1-picture swath	131.63	114.54	4.0	
25	044D31/32	20:40:00	2-picture swath	129.95	136.47	5.4	Control star field
26	044D33/34/35	20:50:00	3-picture swath	94.00	124.65	3.0	Pleiades
27	044D36/37	20:55:00	2-picture swath	94.00	124.65	—[a]	

[a]Camera control word VIS-A 104LG (Exposure = 51 ms).
Camera control word VIS-B 114LG (Exposure = 68 ms).

telemetry, it became evident that pointing errors for both control and knowledge had a slew sign and angle magnitude dependency (hysteresis). Ground calibration suggested that hysteresis effects were present; it was hoped that these effects would be negligible in flight.

(3) The picture pair for the short exposures was intended to analyze internal camera distortion. However, since these pictures remained pointed at the Pleiades, bright stars were visible in the picture and these frames could be used for limit-cycle determination.

3. Analytical Results

a. Hysteresis Model (Knowledge). The Scan Platform pointing software (SCANOPS) had hysteresis model parameters built into its basic structure. However, the hysteresis model had to be added to the original OMSET model to estimate values for these parameters.

b. Hysteresis Model (Control). The control hysteresis was observed to be systematic in nature, i.e., there was a difference in the predicted gimbal angle telemetry and the observed telemetry (DN) that was slew-sign and magnitude dependent.

Hand calculated curves were drawn and the analytic relationships illustrated in Figure 4-4 were incorporated into SCANOPS. Each DN is equivalent to approximately 0.04 deg, thus, as Figure 2-4 illustrates, the control error can contribute as much as 0.16 deg to pointing control error. Since each scan platform step is 0.25 deg, this error is larger than one-half a step, thereby providing the necessary rationale for inclusion in the SCANOPS program. The above model was again verified by examining the Scan Cal II picture sequence predicted and actual telemetry, and shown to be valid.

c. Camera Pointing Control and Knowledge Error Estimates. The pointing results in Tables 4-11 and 4-12 are specified in terms of a camera M, N, L coordinate system where a positive rotation around M decreases the camera clock angle, and a positive rotation around N increases the camera cone angle. The errors are characterized by their standard deviations and extreme values.

The results indicate the 99% requirement for pointing knowledge (0.25 deg) and control (0.50 deg) were met. To provide an indication of what these results mean, a theoretical limit on accuracy can be approximated by considering a simplified model of error sources that cannot be calibrated. This simplified model would consist of the attitude control and scan platform telemetry resolution, which can be considered as uniform random variables. For cone angles near ninety degrees, the spacecraft roll position ($\pm$0.015 deg) and scan platform clock ($\pm$0.02 deg) telemetry uncertainties add, and the resulting distribution would have a standard deviation of 0.014 deg. As the results in Table 4-11 indicate, the Scan Cal I a posteriori statistics are near the limit of removing all nonrandom error sources.

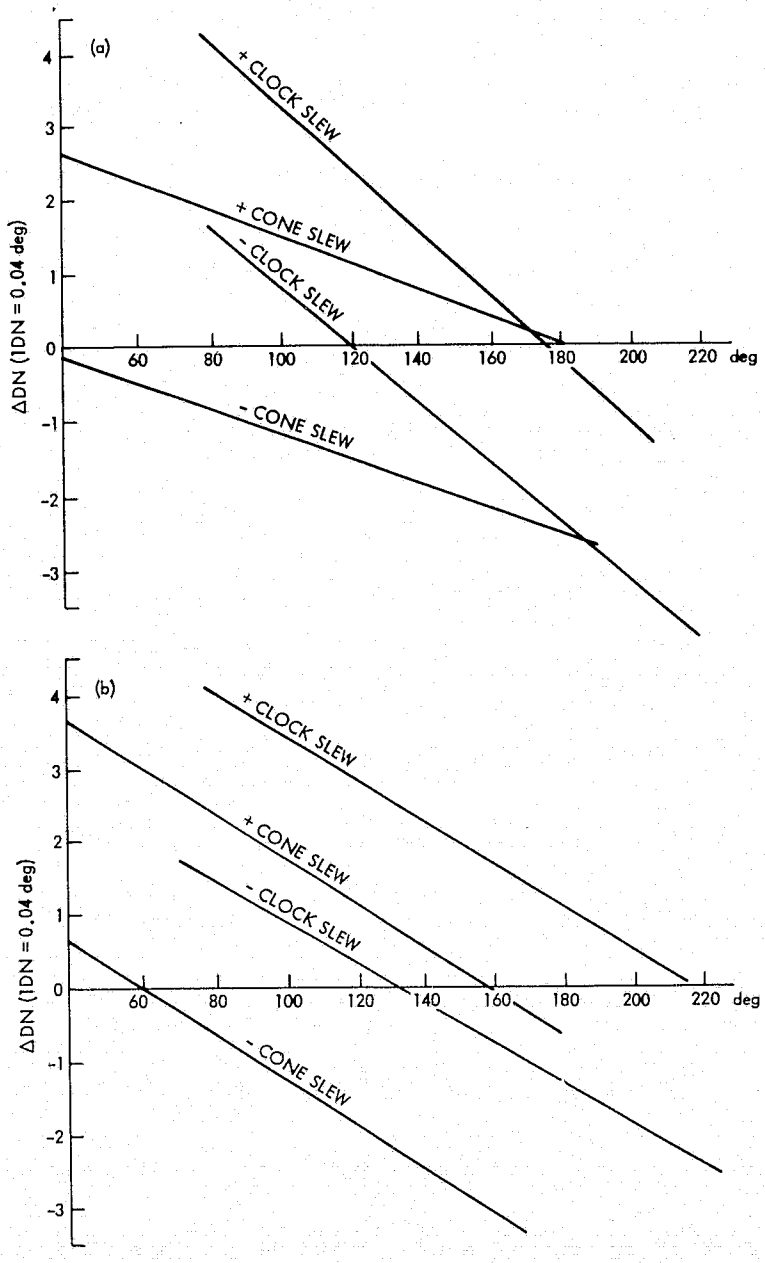

Figure 4-4. Scan Cal I Observed Control Hysteresis: (a) VO-1; (b) VO-2

Table 4-11. Pointing Knowledge Errors (Scan Cal I)

Parameter	Knowledge Error, deg	
	VO-1	VO-2
σ_M	0.019	0.014
σ_N	0.018	0.014
Maximum total error	0.044	0.034

d. Estimated Parameter Set. The estimated parameters in Table 4-13 resulted in the above pointing knowledge errors, and were incorporated into SCANOPS for scan platform pointing computations.

In addition to the Table 4-13 parameters, celestial sensor null offsets were investigated. After the hysteresis parameters were obtained, very little of the pointing error could be accounted for by celestial sensor null offsets. Thus, only scan platform alignment parameters were chosen for the basic parameter set. Subsequent calibrations monitored the celestial sensor null offsets, since changes in the amount of pointing error that can be modeled with sensor offsets would probably be due

Table 4-12. Pointing Control Error (Scan Cal I)

Parameter	Control Error, deg	
	VO-1	VO-2
M	0.166	0.149
N	0.156	0.178
Max M	0.20	0.35
Min N	-0.40	-0.29
Max M	0.30	0.38
Min N	-0.32	-0.40
Maximum total error	0.50	0.49

Table 4-13. Estimated Parameter Set for Knowledge Pointing Errors

Parameter	VO-1	VO-2
Clock gimbal null offset, deg	-0.2016	+0.4553
Cone gimbal null offset, deg	+0.1718	+0.2187
Clock gimbal rotation around a axis, deg	+0.0007	+0.0389
Clock gimbal rotation around b axis, deg	+0.0431	+0.0107
Clock/cone gimbal nonorthogonality, deg	-0.0221	+0.0036
Cone gimbal L nonorthogonality, deg	-0.0117	+0.0057
Scan platform twist around L, deg	-0.0068	-0.06729
Pitch sensor scale factor	-0.0470	+0.0035
Yaw sensor scale factor	-0.0519	-0.0707
Roll sensor scale factor	-0.0229	+0.0236
Clock gimbal mean scale factor	+0.000970	+0.002365
Clock hysteresis differential scale factor	+0.000555	+0.001236
Clock constant hysteresis, deg	+0.0045	-0.0882
Cone gimbal mean scale factor	+0.000232	+0.000683
Cone hysteresis differential scale factor	-0.000145	+0.000642
Cone constant hysteresis, deg	+0.0727	-0.0324

to a change in the sensor characteristics, rather than mechanical alignment changes in the scan platform.

e. Camera Parameters. Along with the above parameter set, the camera alignment with respect to the scan platform was estimated. Table 4-14 shows the in-flight calibration results and compares these to the ground calibrated values.

Table 4-14 points out that the in-flight corrections were less than seven pixels (1 pixel $\approx$ 0.0015 deg) from the ground calibration.

The calibrated values of camera focal length are given in Table 4-15.

The parameters of the "standard camera" for each spacecraft are given in Table 4-16. These are the result of finding the best linear fit to both VIS-A and VIS-B. The 1-σ residuals given indicate the level of agreement between the "standard" and actual camera pictures:

F. SCAN PLATFORM CALIBRATION SEQUENCE II

1. Picture Sequence Design

The second orbiter scan platform calibration sequences were scheduled on Day 103 (4/12/76) for VO-1 and on Day 106 (4/15/76) for VO-2. These sequences consisted of a total of twenty-four pictures each (three

Table 4-14. Camera Alignment (Scan Cal I)

Parameter	Camera Alignment, deg			
	VO-1		VO-2	
	Ground	Flight	Ground	Flight
ψ_A	-0.006	-0.0076	-0.021	-0.0233
X_A	-0.697	-0.7074	-0.684	-0.6793
ω_A	-0.342	-0.2643	-0.233	-0.1193
ψ_B[a]	-0.032	-0.0320	-0.044	-0.044
X_B[a]	+0.681	+0.681	+0.663	+0.663
ω_B	+0.072	+0.0228	-0.427	-0.3362

[a]Nominal values, not estimated.

Table 4-15. Calibrated Camera Focal Length

Viking Imaging System	Camera Focal Length, mm	
	VO-1	VO-2
A	474.59	474.72
B	474.64	474.28

Table 4-16. Standard Camera Parameters

Parameter	VO-1	VO-2
SK:	$\begin{bmatrix} 82.683 & 0.8899 \\ -0.2533 & 82.786 \end{bmatrix}$	$\begin{matrix} 82.529 & 0.8570 \\ 0.0096 & 82.743 \end{matrix}$
(L_{SO}, P_{SO}):	(529.0, 605.0)	(528.6, 604.8)
(σ_L, σ_P):	(1.62, 1.12)	(1.37, 1.42)

four-picture swaths, two three-picture swaths, and six one-picture swaths). The following objectives and considerations were designed into the Scan Cal II sequences:

(1) Hysteresis check by approaching a given region (Mars position) with four different slewing combinations.

(2) Evaluation of Scan Cal I pointing directions that did not seem to conform to models.

(3) Mars pictures used to determine the processing techniques for optical navigation Mars approach pictures.

(4) Playback of star-Mars-star triads immediately at the conclusion of Scan Cal II sequence for a real-time picture processing test by FPAG in preparation for Mars approach optical navigation.

(5) Enough different pointing directions to verify and evaluate models developed from processing of Scan Cal I pictures.

(6) For ease of sequence design keep VO-1 and VO-2 sequences as similar as possible.

(7) Have pictures taken during normal working hours.

(8) Keep number of pictures to a minimum (24 per spacecraft versus the original estimate of 65).

(9) Pleiades four picture swath for camera-to-camera and limit-cycle rate stability analysis.

(10) Exposure verification for Mars image. (Exposure range from 13 to 68 ms).

Tables 4-17 and 4-18 describe the 11 VIS swath events for the 24 VIS pictures; other parameters shown on these tables are Picture Number (103C01 for VO-1, 106D01 for VO-2, etc.), the GMT of shuttering, number of pictures to be recorded, spacecraft scan platform pointing in clock and cone angles, and the VIS camera control words.

2. Optical Navigation Demonstration Test

a. Objectives. Two of the Scan Cal II, star-Mars-star triads (referred to as a "control data type") were used in real time to conduct a test of the techniques for processing optical navigation pictures. In particular, the test results were to determine the feasibility of the critical optical navigation processing requirements. The specific objectives of this test were to:

(1) Demonstrate processing timelines that imply the feasibility of pushing the large volume of picture data through all the concerned agencies (MTC, MTIS, FPAG).

Table 4-17. VO-1 Scan Cal II Picture Sequence

Event No.	Picture No.	Time (4/12/76)	Event	Scan Platform Pointing		Camera Control Words	Notes
				Clock	Cone		
1	103C01/2/3	17:00:00	3-picture swath	127.17	114.94	224.G.[a] 084LG. 224.G.	Star-Mars-star
2	103C04	17:10:00	1-picture swath	109.62	125.61	224.G.	Star
3	103C05/6/7/8	17:20:00	4-picture swath	129.10	115.41	104LG. 224.G. 084LG. 224.G.	Mars-stars-Mars-star
4	103C09	17:30:00	1-picture swath	140.69	125.57	224.G.	Star
5	103C10/11/12	17:40:00	3-picture swath	127.17	114.94	224.G. 084LG. 224.G.	Star-Mars-star
6	103C13	17:50:00	1-picture swath	109.88	106.37	224.G.	Star
7	103C14/15/16/17	18:00:00	4-picture swath	129.10	115.41	064.LG. 224.G. 084LG. 224.G.	Mars-star-Mars-star
8	103C18/19/20/21	18:10:00	4-picture swath	85.75	98.97	224.G. 224.G. 224.G. 224.G.	Pleiades Star-star-star-star
9	103C22	18:20:00	1-picture swath	94.12	115.15	224.G.	Star
10	103C23	18:40:00	1-picture swath	206.26	91.22	224.G.	Star
11	103C24	18:50:00	1-picture swath	185.07	92.16	224.G	Star

[a]Control Word EEFLGO: EE = Exposure (22 = 2.66 s)
F = Filter (4 = clear)
L = Light Flood (. = no L.F.)
G = High Gain
O = DC Offset (. = off)

Table 4-18. VO-2 Scan Cal II Picture Sequence

Event No.	Picture No.	Time (4/15/76)	Event	Scan Platform Pointing		Camera Control Words	Notes
				Clock	Cone		
1	106D01/2/3	17:00:00	3-picture swath	116.48	107.96	224.G.[a] 084LG. 224.G.	Star-Mars-star
2	106D04	17:10:00	1-picture swath	108.30	122.58	224.G.	Footnote b
3	106D05/6/7/8	17:20:00	4-picture swath	118.27	107.94	114LG. 224.G. 084LG. 224.G.	Mars-stars-Mars-star
4	106D09	17:30:00	1-picture swath	138.39	123.40	224.G.	Footnote b
5	106D10/11/12	17:40:00	3-picture swath	116.48	107.96	224.G. 084LG. 224.G.	Star-Mars-star
6	106D13	17:50:00	1-picture swath	108.93	103.35	224.G.	Footnote b
7	106D14/15/16/17	18:00:00	4-picture swath	118.27	107.94	074.LG. 224.G. 084LG. 224.G.	Mars-star-Mars-star
8	106D18/19/20/21	18:10:00	4-picture swath	85.10	95.85	224.G. 224.G. 224.G. 224.G.	Footnote b Star-star-star-star
9	106D22	18:20:00	1-picture swath	104.00	65.64	224.G.	Star
10	106D23	18:40:00	1-picture swath	205.47	92.47	224.G.	Star
11	106D24	18:50:00	1-picture swath	184.26	92.27	224.G.	Footnote b

[a]Control Word EEFLGO: EE = Exposure (22 = 2.66 s); F = Filter (4 = clear); L = Light Flood (. = no L.F.); G = High Gain; O = DC Offset (. = off)

[b]Same star field as VO-1.

(2) Demonstrate a processing rate for OMSET of 3 pictures every two hours.

(3) Demonstrate the overall integrity of the ground data system, particularly the consistency of the OMSET/ONP interface.

(4) A medium by which the OMSET personnel could familiarize the Interplanetary Determination Team (IPODT) personnel with uplink procedures.

b. Results - Problems and Actions Taken. The timeline performance for the first triad processing clearly indicated the feasibility of the planned orbit determination timelines for the optical navigation portion of the control and knowledge approach phases.

Problems were encountered during the processing of the second triad. The VIS SDR was not processed immediately upon receipt due to some confusion caused by the appearance of science requests for this picture. As a result of this delayed processing, important steps were taken within the Viking Flight Team to insure that optical navigation processing would have priority for processing.

During this test it became apparent that the OMSET processing procedures for handling engineering telemetry were inefficient, subject to error, and consuming too much time. Additional software was developed (AUTOFLY and TRANS.), and new processing procedures were established for application to the actual optical navigation processing.

3. Camera Pointing Control and Knowledge Error Estimates

The error parameter sets estimated in Scan Cal I (Section V-C) were used. The pointing results in Tables 4-19 and 4-20 are specified in camera M, N, L coordinates and the errors are characterized by their standard deviations and extreme values. The results indicate that the 99% requirements for pointing knowledge (0.25 deg) and control (0.50 deg) were still being met. Items of interest are that the pointing knowledge errors in the cone direction (N) appear to be more consistent with the Scan Cal I results, while the pointing knowledge errors in the clock direction (M) seem to be larger than the formal statistics from Scan Cal I (σ_m = 0.018 deg VO-1 and σ_m = 0.014 deg VO-2). Attempts were made to isolate an error parameter change (e.g., celestial sensor offsets) to account for this change; however, nothing conclusive resulted. Also, the pointing for VO-2 picture number 106D23, which was at a clock angle greater than 180 degrees, does not seem to conform to the current models. This picture is in the same scan platform region where picture 44D04 (VO-2) was taken, and the pointing for 44D04 has never been resolved. The trends on VO-2 indicated that, once the lander is separated and high clock angles become available, the extended region should be calibrated to insure meeting the pointing knowledge requirements.

Table 4-19. Scan Calibration II Results (VO-1)

Parameter	Pointing Knowledge Error, deg		Pointing Control Error, deg	
	M	N	M	N
Mean	-0.014	+0.003	-0.03	0.012
σ	0.029	0.010	0.15	0.12
Maximum	0.030	0.013	0.23	0.14
Minimum	-0.062	0.022	-0.35	-0.24
Maximum total error	0.063		0.36	

Slight changes (subpixel) from the camera-to-camera alignment determined in Scan Cal I seemed to be present, more so for VO-2 than VO-1. However, for scientific purposes, pointing was well within the requirements. Consequently, it was recommended that SCANOPS continue with the same parameter sets determined in Scan Cal I.

As a result of the apparent slight shift in camera-to-camera alignment, it was recommended that, prior to the optical navigation picture sequences, a star triad be taken to again reexamine camera alignment.

Table 4-20. Scan Calibration II Results (VO-2)

Parameter	Pointing Knowledge Error, deg[a]		Pointing Control Error, deg	
	M	N	M	N
Mean	-0.022 (-0.012)	0.022 (0.006)	0.07	0.04
σ	0.038 (0.025)	0.025 (0.023)	0.17	0.12
Maximum	0.044 (0.044)	0.044 (0.044)	0.32	0.33
Minimum	-0.114 (-0.052)	0.039 (-0.022)	-0.23	-0.20
Maximum total error	0.120 (0.057)		0.40	

[a]Numbers in parenthesis are without picture 106D23.

4. Mars Picture Processing

The star-Mars-star triads were extensively used to investigate the best ways to process optical data. Four important Mars center finding improvements were made:

(1) Limb points should be given more weight in the estimation process.

(2) The 10% above threshold (background) is a better level than 50% to determine limb points.

(3) Several levels of data editing should be used to determine the quality of the center finding process.

(4) A 12-ms exposure should be used for Mars.

All of the above procedures were adopted and used throughout all the optical navigation Mars pictures.

Tables 4-21 and 4-22 show the computed Mars residuals for different processing techniques. The results in these tables indicate that extremely high accuracy can be achieved especially in the pixel direction (the R direction in the B plane, which is not well determined by radio data). As will be shown in latter sections, this indeed was the case, and, surprisingly enough, the actual navigation line residuals were better than the Scan Cal II line residuals and, in fact, were more consistent with the pixel accuracies.

G. SCAN PLATFORM CALIBRATION SEQUENCE III

1. Picture Sequence Design

During the approach optical navigation pictures, the scan platform offset in the cone direction changed approximately -0.15 deg on VO-1 after the Mars approach trajectory correction maneuvers. This offset was conjectured to have been introduced as a result of not moving the platform against the stops prior to the maneuver. All subsequent maneuvers were done with the platform near the stops for both orbiters, and no new negative offsets were observed. Scan Cal III was primarily designed to verify scan platform alignment after the large Mars orbit insertion engine burn, and not for calibration purposes. These sequences consisted of just a few pictures spaced throughout the available scan platform region.

2. Results

Scan III for VO-1 occurred on day 189, and the results of processing these three pictures are given in Table 4-23.

Table 4-21. VO-1 Mars Processing Results

Picture No.	Camera	Exposure, ms	Mars Line and Pixel Residuals (Observed - Expected)					
			Method 1[a]		Method 2[b]		Method 3[c]	
103C02	B	25	-0.46	0.25	-0.60	0.40	-0.76	0.26
103C05	A	50	-0.55	-0.41	-0.93	-0.58	-1.35	-0.31
103C07	A	25	-0.99	-0.16	-1.38	-0.33	-2.12	-0.29
103C11	B	25	-1.23	-0.06	-1.14	-0.15	-1.16	-0.07
103C14	A	12	0.77	0.61	0.22	0.36	0.05	0.66
103C16	A	25	-0.69	0.30	-1.23	0.06	-1.96	-0.06
		Mean	-0.52	0.09	-0.84	-0.04	-1.22	0.03
		σ	0.63	0.34	0.54	0.35	0.73	0.34

[a]Camera distortion calibrated--stars and telemetry weighting normal.

[b]A priori distortion model--stars and telemetry weighting normal.

[c]Camera distortion calibrated telemetry deweighted.

Table 4-22. VO-2 Mars Processing Results

Picture No.	Camera	Exposure, ms	Residuals[a]	
			Line	Pixel
106D02	B	25	-1.49	-0.27
106D05	A	75	-1.51	0.63
106D07	A	25	-1.69	0.84
106D11	B	25	-1.00	0.00
106D14	A	18	-0.99	0.98
106D16	A	25	-1.94	0.98
		Mean	-1.44	0.53
		σ	0.53	0.69

[a]Camera distortion based on 106D10/11/12.

Table 4-23. Scan Cal III Mars Processing Results (VO-1)

Picture No.	Telemetry Determined[a] Pointing, deg		Actual (STAR) Pointing, deg	
	Clock	Cone	Clock	Cone
189A01	119.593	110.981	119.599	111.034
189A02	90.049	93.807	90.041	93.865
189A03	170.035	102.643	169.953	102.687

[a]Processed with -0.15 deg cone offset observed in approach pictures.

These results demonstrate that the pointing knowledge was less than 0.1 deg, and the negative cone bias observed in approach appears to be reduced to -0.10 deg.

On revolution 4 (day 224) for VO-2, six star frames were taken to verify the existing scan platform alignment model parameters used in pointing control and knowledge computations for the scan platform. The results of processing these six pictures were:

Pointing Knowledge, deg:

	Cone	Cross Cone
Mean	0.01	0.00
Sigma	0.01	0.04

Max. total pointing error: 0.064

Pointing Control, deg:

	Cone	Cross Cone
Mean	0.00	0.06
Sigma	0.16	0.14

Max. total pointing error: 0.32 deg

These results indicate the pointing for VO-2 had not been affected by Mars orbit insertion, and that both the camera pointing control and knowledge were well within the requirements of 0.5 and 0.25 deg.

H. SCAN PLATFORM CALIBRATION SEQUENCE IV

1. Picture Sequence Design

Scan Cal IV was designed to help characterize any offsets introduced in orbit by engine burns and, primarily, to provide calibration parameters that apply over the entire scan platform region, which had been significantly increased after the lander was separated. Also, a scan platform pointing was investigated where high rate slews (1 deg) were used to point the scan platform. Table 4-24 describes the picture sequence for VO-1. Scan Cal IV was cancelled on VO-2 because the bioshield base cover was left attached to the orbiter, which prevented the scan platform from using the extended region.

2. Results

Table 4-25 contains the results of processing the engineering telemetry using the existing calibration model parameters. Table 4-26 contains the results with an updated value for five of the sixteen parameters determined in Scan Cal I.

Table 4-24. Scan Cal IV Pictures

Picture No.	Desired Camera Pointing, deg		Telemetry Determined Pointing, deg		Actual (STAR) Pointing, deg	
	Clock	Cone	Clock	Cone	Clock	Cone
004Y01	144.21	120.27	144.01	120.21	143.95	120.22
004Y02	166.35	102.64	166.38	102.75	166.44	102.77
004Y03	116.49	99.04	116.32	99.23	116.35	99.23
004Y04	115.22	137.71	115.19	137.52	115.20	137.55
004Y05	90.16	78.49	90.34	78.58	90.34	78.58
004Y06	106.78	108.48	106.55	108.29	106.50	108.30

Table 4-25. Pointing Knowledge Error (Existing Parameter Set)

Parameter	Pointing Knowledge Error, deg		
	Mean	Sigma	Max.
Cross cone	-0.021	0.070	+0.13
Cone	+0.097	0.033	+0.16
Maximum total pointing knowledge error			0.18

Based on the results of Scan Cal IV, the following change in parameter value was recommended for use in SCANOPS for VO-1 to improve pointing knowledge for the full-scan platform region:

Table 4-26. Updated Values in Scan Cal I

Parameter	Old	New
Cone gimbal null offset, deg	+0.0218	+0.1217
Clock gimbal null offset, deg	-0.2016	-0.3362
Clock constant hysteresis, deg	+0.0045	+0.0605
Clock gimbal mean scale factor	+0.000970	+0.000045
Clock hysteresis differential scale factor	0.000555	+0.000473

The -0.15 deg cone null offset induced by approach motor burns appeared to be reduced to approximately -0.05.

Based on all celestially referenced VO-1 star pictures (327 frames) taken since the near Earth calibration sequences, the pointing knowledge requirement of 0.25 degrees was still being achieved.

SECTION V

OPTICAL NAVIGATION

A. INTRODUCTION

Originally the optical navigation sequences were to consist of a series of pictures at encounter minus 33 days (E-33), E-13 days, E-72 hours. The pictures taken at E-33 and E-13 were referred to as "control" pictures and used Mars as the observable, while the pictures at E-72 hours were referred to as the "knowledge" pictures and used the Mars satellite Deimos as the observable. However, as a result of the success of processing the departure Earth and scan platform calibration Mars pictures, it was recommended to include "control"-type pictures after the near-Mars maneuvers. The merits of making this decision were clearly demonstrated when VO-1 developed a leak in a propellant regulator valve and required several near-Mars maneuvers to reduce pressure. The added control-type pictures spread over a longer time arc resulted in very accurate trajectory estimates. In fact, as a result of the success on VO-1 using the longer arc data, additional control pictures were designed for VO-2. The Viking mission was the first time a two-camera technique was used for optical navigation, as well as the first time optical data was used in operationally determining trajectories and maneuver strategies.

The following schedule Table 5-1 reflects the observation times and the number of pictures used for approach optical navigation.

B. NAVIGATION OBSERVATIONS

1. Control

The "control" data type consisted of three successive pictures spanning a period of three frame times (13.44 s). These pictures consisted of a long (2.66 s) exposure star frame, a short exposure (0.012 s) picture of Mars, and finally a long exposure star frame. Originally, the concept was to use the A camera for the star frames. However, based on the VO-2 Scan Cal II apparent camera-to-camera misalignment signature in the Mars residuals, and the fact that available stars were on either side of Mars, it was recommended that the cameras be alternated in each successive triad. By taking BAB and ABA (Figure 5-1), triad differences of camera response, as well as camera alignments, can be readily detected.

For either the BAB or the ABA triad, as illustrated in Figure 5-1, the star frames are used to estimate the "best" pointing of the middle of the exposure of the Mars frame where the relative camera alignment is known. Since the position of stars is essentially invariant for different trajectory positions, any image displacement of Mars is considered to be predominately trajectory error. The other error sources that can contribute to Mars' residuals are:

Table 5-1. Schedule for Approach Optical Navigation

Event	Date of Picture Sequence Start	Day No.	Spacecraft	Time to Encounter, days	No. of Pictures
Control I	5/17/76	138	VO-1	34	54
Control II	6/3/76	155	VO-1	17	54
Control III	6/10/76	162	VO-1	10	24
Knowledge	6/16/76	168	VO-1	4	26
Control I	7/7/76	189	VO-2	31	36
Control II	7/16/76	198	VO-2	22	36
Control III	7/22/76	204	VO-2	16	36
Control IV	7/28/76	210	VO-2	10	36
Knowledge	8/2/76	215	VO-2	5	24
	Total navigation pictures				326
	Total information processed				(3.1 X 10^9 bits)

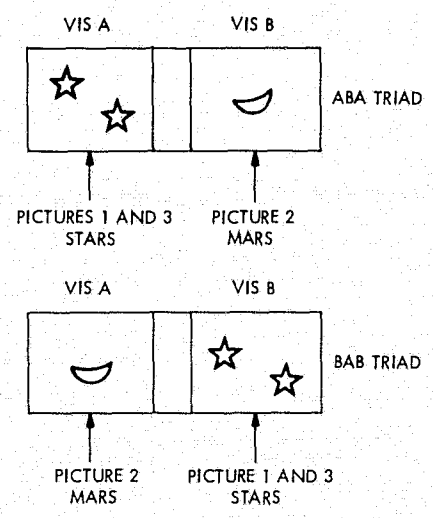

Figure 5-1. Control Triads

(1) Camera-to-camera alignment error.

(2) Limit-cycle estimation error.

(3) Star camera pointing error.

(4) Mars center finding.

The first three of these error sources tend to reduce in magnitude as the number of stars in the picture increases. The effect of the Mars center finding error on trajectory miss in the B-plane is minimized if:

(1) Error is constant (bias).

(2) Data arc is long enough to separate out bias errors.

Because of the Mars approach geometry restrictions and spacecraft Sun-Canopus referencing, there is a very good relationship between the camera MNL coordinates and the B-plane RST coordinate system. As Figure 5-2 illustrates, the line direction corresponds to the $\hat{T}$ direction and the pixel direction corresponds to the $\hat{R}$ direction. Thus, to first order, residuals in line correspond to T errors and residuals in pixel to R errors. A simplified model to estimate errors in the B-plane becomes:

$$-\Delta l * 25 \times 10^{-6} = \frac{\Delta B \cdot T}{R} + \frac{\Delta V \cdot T}{V_\infty} + C_l$$

$$\Delta p * 25 \times 10^{-6} = \frac{\Delta B \cdot R}{R} + \frac{\Delta V \cdot R}{V_\infty} + C_p$$

where:

Δp = Mars pixel residual

Δl = Mars line residual

$\Delta B \cdot T$ = miss in T direction

$\Delta B \cdot R$ = miss in R direction

$\Delta V \cdot T$ = velocity error in T direction

$\Delta V \cdot R$ = velocity error in R direction

V_∞ = approach velocity

C = center finding error

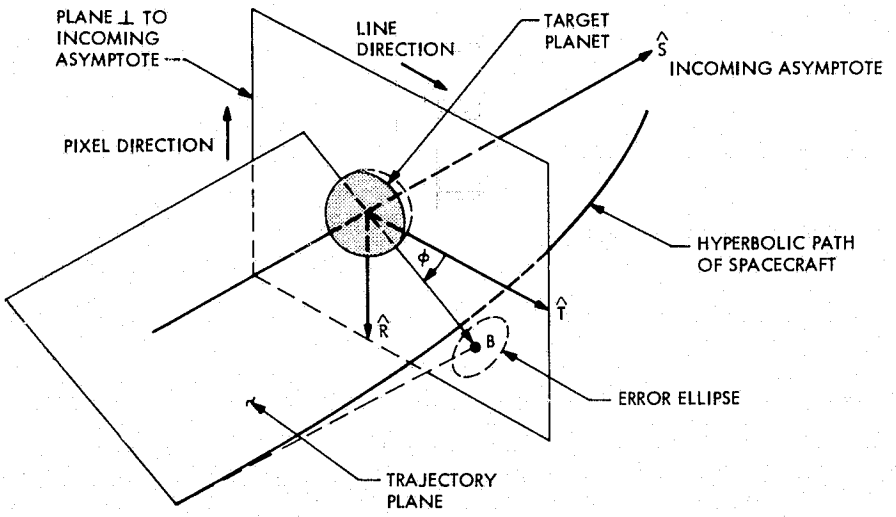

$\hat{S}$ = INCOMING ASYMPTOTE
B = MISS PARAMETER (B ⊥ $\hat{S}$)
$\hat{T}$ = PARALLEL TO ECLIPTIC PLANE AND ⊥ TO $\hat{S}$
$\hat{R} = \hat{S} \times \hat{T}$

V_∞ = VELOCITY AT INFINITY
T_F = LINEARIZED TIME OF FLIGHT
SMAA = SEMIMAJOR AXIS OF ERROR ELLIPSE (1σ)
SMIA = SEMIMINOR AXIS OF ERROR ELLIPSE (1σ)

Figure 5-2. B-Plane and Line-Pixel Orientation

The above equations show that a constant center finding error is indistinguisable from a velocity error. However, maneuver computations are designed to correct miss, thus velocity and/or constant center finding are not important provided the dynamic range (ΔR) is enough to separate them. Knowing that constant errors in Mars center are not detrimental dictated the need for consistent processing strategies for all control pictures.

2. Knowledge

The "knowledge" observations are single-frame pictures of Deimos and a star background. These pictures are long exposure and suffer from the problem that the basic navigation observable (Deimos) is overexposed, i.e., image "blooming," "smearing," and "spreading". All of these error sources make image centerfinding difficult for the Deimos image. The fact that the range is greatly reduced for the Deimos pictures minimizes the significance of these error sources in terms of kilometers of trajectory errors. However, as the results of the following sections show, purely on a pixel measurement basis, the knowledge data type contains more random noise than the control observations.

3. Calibration

The scan platform calibration sequences discussed in the previous section of this report calibrated various error models for the spacecraft attitude control system, scan platform and VIS. The results of these calibrations and processing of Mars and Earth pictures directly affected the success of processing optical navigation data. In particular, these calibration activities determined:

(1) Camera-to-camera alignment: necessary for the control navigation pictures to properly determine the pointing of the Mars frame that contains no stars.

(2) VIS geometric distortion (optical, electromagnetic, and raster): necessary to provide image locations corrected for distortion, as well as accurate pointing and images for the trajectory estimation.

(3) Camera pointing control, error estimate: required to determine picture pointing strategies and optimize the probability of satisfactory data return.

(4) VIS sensitivity: Star magnitude detection capability and Mars image response necessary for pointing strategy of star frames and exposure settings for the Mars image.

(5) Accurate pointing knowledge from engineering telemetry: required to generate predicted star positions and assist in the rapid data reduction of the volume of digital information contained in a single picture (9.5×10^6 bits).

(6) Mars centerfinding parameters: limb detection techniques and data weight necessary for consistent, accurate center estimation.

The accurate pointing knowledge from engineering telemetry is most important for the navigation control triads, since stars, in general, do not provide the most accurate determination of camera rotation. For example, two stars separated by 500 pixels with a 1-pixel (1σ) location accuracy determine rotation to an accuracy of 0.16 deg (1σ), while engineering telemetry can approximate accuracies on the order of 0.01 deg (1σ). To determine the significance of a rotation error on the expected location for Mars or Deimos, the distance from the centroid of the stars to the object times the rotation error approximates the error in a Mars or Deimos location. Thus, engineering telemetry is very important to control pictures, since the Mars-to-star centroid distance is, in general, large. A good calibration and use of engineering telemetry will result in consistent and accurate line locations for the expected Mars image.

C. NAVIGATION MEASUREMENT PROCESSING

1. Sequence Design - Pointing Optimization

Picture times for all the optical navigation were, to a large part, selected as a junction of operational constraints (DSN availability, sequence design scheduling, spacecraft operations, etc.). The most critical picture time selection was for the Deimos pictures, which should provide a representative coverage of mean anomalies for Deimos. For the control triads, both the ABA and BAB type, the star-Mars geometry does not appreciably change over a few days, so picture time is not important other than to provide a fairly long and uniform time spread of pictures for bias removal (velocity and/or Mars center). The times for all pictures were transmitted to OMSET via the Picture Sequence Data file (PSDF). This file was used as input to the Probability of Stars Evaluation (POSE) program, which optimizes picture pointing. Specifically, POSE, for a given control picture time, determines the scan platform pointing for a given pointing error that:

(1) Guarantees Mars will not appear in the long exposure star frame.

(2) Maximizes the number of detectable stars in the star frame.

Similarly, for knowledge, POSE determines the scan platform pointing that:

(1) Guarantees Mars will not appear in the Deimos Frame.

(2) Subject to condition one, optimizes the pointing to guarantee acquisition of Deimos.

(3) Maximizes the number of detectable stars.

The pointing direction delivered to the sequence planners was the optimum pointing corrected for gimbal null offsets, hysteresis, and command resolution. The command value and channel were selected as close to the optimum as possible, while not violating the constraints listed above.

2. Data Flow and Management

Many Viking Flight Team organizations were involved in the scheduling and processing of navigation pictures. A large volume of pictures was processed with relatively few problems as a result of two important decisions:

(1) Optical navigation data were managed directly by the people processing the data, rather than the normal procedures for science pictures.

(2) The Mission Integration Working Squad (MIWS) was instructed to give navigation priority over all other video processing requests.

Table 5-2. Processing Flow for Raw Picture Data

Event	Data Type	Time, min
Triad recorded at spacecraft		T
Triad received at SFOF	VIS SDR tape	T + 80
Video reconstructed	VIS EDR tape	T + 140
Optical measurement processing complete	OMSET data file available	T + 200

The events and times given in Table 5-2 depict a typical processing flow for the raw picture data for a control navigation triad played back at 8 kbps.

Conditions that caused deviation from this nominal schedule were:

(1) 1108 problems.

(2) Delays in the reconstruction process.

(3) Bad tapes.

Fortunately, the above occurred for less than 10% of the pictures processed.

3. Telemetry Data Processing

For optical navigation pictures, no time was available to obtain telemetry from the normal processing path, i.e. TDRP, SCANOPS, etc. This fact became apparent during the preliminary processing tests during the Scan Cal II sequence. To circumvent these unacceptable time delays, a program (AUTOFLY) was written to dump the engineering telemetry from the flyback information on the reconstructed video data. Flyback data is information that is recorded on the spacecraft during the time the vidicon scan readout beam is returning. This amounts to 542 bits of information for each line of a picture. Because the information is laid down on each of the seven tracks of the flight tape recorder, it becomes seven times redundant data. All the engineering measurements were contained within this flyback. The first step in the optical measurement processing was to use AUTOFLY and dump the engineering telemetry measurements (pitch, yaw, roll, scan platform clock, and cone) from the VIS EDR. These telemetry measurements were then used to predict where the picture was taken and generate the expected position, in

camera coordinates, where images should appear. A basic formatted input file for the pointing estimation process was created based on just engineering telemetry. Once the location of an actual image was determined (usually Mars and Deimos) in the hard copy picture, translations from the engineering predicts were determined in Δ lines and Δ pixels.

4. Picture Data Processing

a. Star Images. The above line and pixel translations of the engineering predicted star locations were input to a program (TRANS) that automatically constructed an input file used to dump selected areas of the raw video data thought to contain star images. From the computer printout of the picture intensities (DN levels), the line and pixel location of the peak intensity was determined for the star image. Selection and rejection criteria had to be applied to account for missing tape recorder tracks that were filled with adjacent pixel information, noise spikes, and shutter or filter step-induced microphonics. Once a valid star location was determined, the predicts file was edited with the actual location for each star.

b. Mars Image. The Mars image center was determined by fitting a set of limb points by an ellipse. The ellipse eccentricity and orientation in camera coordinates was constrained to the eccentricity and orientation that result from mapping to camera coordinates, the equatorial and polar radii of Mars. The Mars limb points were determined by scanning the region of the picture containing Mars along a constant pixel (vertical) direction and finding the interpolated line location where the Mars image signal was 10% above the mean background signal level. This interpolation signal level (threshold) varied from camera to camera. However, the threshold level was held fixed for each individual camera throughout all control Mars pictures. The line and pixel location for the center of the ellipse fitted to the limb points was used as the observed location for the center of mass for Mars. Since all Mars pictures were taken at a 12-ms, exposure, the images were not overexposed or smeared and of good quality for obtaining a consistent set of center estimations. Because of the crescent shape of the Mars image (phase angle $\approx$ 120 deg) and orientation within the picture, the pixel location for the center was more accurate than the line location. No matter what reasonable variations were tried in preliminary studies to determine the Mars center the pixel location was virtually invariant. This was a comforting fact, in that a high confidence was always placed on the pixel location of Mars; this location was the most important measure to complement radio information because the pixel direction corresponds to the R direction in the B plane. Surprisingly enough, the Mars line locations correlated well with radio data and, indeed, was almost as accurate as the pixel locations.

c. Deimos Image. The observed and pixel location of Deimos was determined by hand processing the computer printout of the intensity levels in the vicinity of the Deimos image. Preflight studies on ways

to improve upon the MM'71 Deimos center finding technique showed that "boxing" was a consistent technique for center determination. Boxing entails determining a rectangle drawn around the Deimos image where the sides of the rectangle are drawn just before the first observed signal appears above the mean background. The center of the box is used as the estimate for the observed center of mass for Deimos. This technique has the advantage that it is least subject to errors due to beam pulling, and provides a systematic procedure for locating Deimos

d. Reseau Images. Reseau images were used to determine the distortion calibration parameters (Section II-B) necessary to remove internally induced camera distortion. Reseau images on the edge of the vidicon, as well as the first line (lowest line No.) were not used for distortion calibrations. The former were omitted since the ground measured X-Y millimeter coordinates were not as accurate as those for internal reseaux, and the latter were omitted due to the highly nonlinear response that was observed in preflight studies to occur for approximately the first sixty lines. By using only the internal reseaux, an excellent calibration was possible for the region where images would be processed for camera pointing estimates.

Special software was developed for Viking to do the following calibration process:

(1) Writing a file of 7 x 7 areas around the a priori reseau locations that were determined for each vidicon serial number from ground calibrations.

(2) For each of these 7 x 7 areas, the local minimum response (with suitable acceptance-rejection logic for missing data and noise spikes) was determined by using two-way quadratic interpolation. This interpolated minimum point was used as the observed reseau location to estimate the distortion parameters.

(3) The extracted locations were then placed on an internal file that was then automatically accessed by the OMSET calibration routines.

Prior to Viking, camera calibrations were tedious in nature because a large amount of manual interface was required. The time factor for a single camera calibration was reduced from several hours to less than ten minutes, and at no time did any of the automatic calibrations misidentify any reseau locations.

5. Navigation Observation Generation

The residuals from processing the star, target (Mars or Deimos), and engineering telemetry were evaluated, and each image was accepted, rejected, and/or reevaluated until a consistent set of data remained. In general, star images were rejected because they were either too bright (beam pulling), near the edge of the field-of-view, or incorrectly

identified. The Mars center estimate chosen was the location which, along with an edited set of limb points, produced the lowest residual statistics in fitting the limb points with an ellipse.

The processing of the stars-Mars-stars triad consisted of estimating the VIS pointing error and attitude control rates based on engineering telemetry and the star images in the first and third pictures. Then, by using the estimated pointing directions, attitude control rate, and the camera-to-camera alignment, the pointing direction at the middle of the exposure window for the Mars picture was determined. For the Deimos star picture only the pointing direction was estimated since only a single frame was used as an observation.

As each observation was processed it was added to the OMSET data file, which was used as the interface file to pass data for trajectory estimation. This file contained miscellaneous picture, image, and processing parameter identification. However, the primary information passed and used for trajectory determination was:

(1) The "best estimate" of pointing for a distortionless camera containing the observable (Mars/Deimos).

(2) The "best estimate" of the observable location (line and pixel) in this distortion-free camera.

D. PROCESSING RESULTS

1. Camera Pointing

The success of the pointing optimization process and the operation of the scan platform was clearly demonstrated in that one of the three-hundred and twenty-six optical navigation pictures was unuseable because of missing the target or stars. One anomaly did develop on VO-1 that resulted in a slight degradation in camera pointing. Prior to the first approach midcourse maneuver (AMC1), the scan platform exhibited a very small cone offset ($\approx$0.02 deg) based on the series one and two optical navigation pictures. After AMC1 ($\approx$ 50 m/s) the scan platform had a -0.075 deg cone offset based on the series three optical navigation pictures. After AMC2 ($\approx$60 m/s), the scan platform exhibited a -0.13 deg cone offset. These offsets were attributed to the fact that the scan platform was not lowered to the stops in the stow position prior to motor burns. All subsequent maneuvers for both VO-1 and VO-2 were done with the scan platform lowered and no new negative cone offsets were observed. In fact, the negative offset on VO-1 was observed to be reduced by approximately half its value after the Mars Orbit Insertion burn (MOI). Table 5-3 summarizes the scan platform pointing knowledge error (star-determined pointing minus pointing from engineering telemetry) for all the approach optical navigation picture sequences.

Table 5-3. Pointing Knowledge for Approach Navigation Pictures

Spacecraft	Picture Series	Pointing Error			
		Mean/Sigma		Mean/Sigma	
		Lines	Pixels	Cone, deg	X-Cone, deg
VO-1	Control No. 1	14.0/13.1	11.1/26.5	0.02/0.02	0.02/0.04
	Control No. 2	12.4/9.9	1.8/18.7	0.02/0.01	0.00/0.03
	Control No. 3	-55.9/12.0[a]	12.0/23.4	-0.08/0.02	0.02/0.03
	Knowledge	-91.1/16.0[a]	-7.4/17.5	-0.13/0.02	-0.01/0.03
VO-2	Control No. 1	10.2/10.9	18/11.9	0.01/0.02	0.03/0.02
	Control No. 2	19.9/9.5	-1.0/17.0	0.03/0.01	0.00/0.02
	Control No. 3	4.8/9.8	6.0/7.8	0.01/0.01	0.01/0.01
	Control No. 4	3.9/19.2	14.5/8.9	0.01/0.02	0.02/0.01
	Knowledge	-	-	-	-

[a]Negative cone offset induced by motor burn.

2. Mars and Deimos Residual Statistics

After processing the first series of control triads for each orbiter, a very definite pattern in the Mars residuals resulted. The residuals for Mars in VIS A were different from those in VIS B by about a third of a line and pixel for VO-1 and a third of a line and one pixel for VO-2. Naturally, the rotational orientation of each camera was slightly different (as much as 0.8 deg), which would cause a difference in the line and pixel residuals (tan Δ rotation x Mars residual). However, for the small Mars residuals experienced during the first control series, this effect would be less than one tenth of a pixel. This alternating signature could be the result of any one or a combination of the following:

(1) Camera-to-camera alignment wrong.

(2) Different response of A and B camera to Mars image.

(3) Camera systematic center finding error.

Knowing that this signature should not be present, it was decided to use the Mars image and solve for a set a scan platform and camera rotations

that smoothed out the Mars residuals in the first control series (referred to as the "ferris wheel" effect). Once a new set of evaluations was determined, it was applied to all subsequent control pictures. Since star triads were available to check camera-to-camera alignment, both prior to and after the navigation pictures, they tended to indicate the camera-to-camera alignment was good for stars, thus hinting at a changing camera response to the Mars image as the cause of alternating residuals. In any event, no matter what set of offsets was used, the mean Mars line and pixel residual over a given series of pictures was not appreciably changed, and this is the primary factor influencing the trajectory solution. Table 5-4 contains the updated camera parameters, and Table 5-5 sumarizes the "scatter" in residuals for various processing conditions; all residuals were not fit with a trajectory unless indicated and are thus conservative.

As the results of Table 5-5 indicate, the optical navigation measurement accuracy appears to be on the order of a third of a line and a pixel, one sigma. This performance was far better than hoped for before launch, where estimates varied from one to two pixels, one sigma.

E. CONCLUSIONS AND RECOMMENDATIONS

The success of the approach optical navigation was a direct result of the integrated approach of combining scan platform calibration sequences with optical navigation picture processing studies. These studies provided the necessary experience to be totally prepared to handle the large volume of navigation pictures on a time-critical schedule. Although there are many areas where the processing procedures can be automated to reduce the amount of manual operations required to process optical data, it does not appear that much improvement in accuracy is possible. In fact, a completely automated approach may degrade the accuracy because of the large number and variety of real-time processing decisions that were made by the personnel processing the optical data.

Table 5-4. Updated Camera Alignment Used for Mars Pictures

Camera Alignment	Offset Parameter, deg						
	ψ_A	χ_A	ω_A	ψ_B	χ_B	ω_B	ω_P
VO-1 a priori	-0.0076	-0.7074	-0.2643	-0.032	0.681	0.0228	-0.0068
VO-1 updated	-0.0076	-0.7074	-0.2663	-0.032	0.681	0.0884	-0.0064
VO-2 a priori	-0.0233	-0.6793	-0.1193	-0.044	0.6630	-0.3362	-0.0623
VO-2 updated	-0.0236	-0.6799	-0.2045	-0.044	0.6631	-0.2483	-0.07111

$\psi_{A,B}$ = Cone offset (camera A and B)

$\chi_{A,B}$ = Cross cone offset

$\omega_{A,B}$ = Rotation

ω_P = Scan platform rotation

Table 5-5. Mars/Deimos Residual Summary

Spacecraft	Series	Number of Observations	Line	Pixel
VO-1	Control No. 1	17	0.47	0.31
	Control No. 1[a]	17	0.36	0.19
	Control No. 2	18	0.22	0.28
	Control No. 3	8	0.75	0.26
	Control No. 3[b]	8	0.34	0.20
	Knowledge[c]	26	1.08	0.74
	Knowledge[d]	26	0.26	0.43
VO-2	Control No. 1	12	0.27	0.64
	Control No. 1[a]	12	0.27	0.26
	Control No. 2	12	0.33	0.29
	Control No. 3	12	0.32	0.45
	Control No. 4	12	0.41	0.39
	Knowledge[e]	23	0.65	0.49
	Knowledge[d]	23	0.38	0.37

[a]"Ferris wheel" effect removed (see Table 5-4).
[b]Fit with a trajectory.
[c]Preflight Deimos ephemeris used.
[d]Residuals with a trajectory and ephemeris fit to data.
[e]VO-1 Deimos ephemeris used.

TECHNICAL REPORT STANDARD TITLE PAGE

1. Report No. JPL Pub. 77-28	2. Government Accession No.	3. Recipient's Catalog No.
4. Title and Subtitle Calibration of Viking Imaging System Pointing, Image Extraction, and Optical Navigation Measure		5. Report Date September 15, 1977 6. Performing Organization Code
7. Author(s) W. G. Breckenridge/J. W. Fowler/E. M. Morgan		8. Performing Organization Report No.
9. Performing Organization Name and Address JET PROPULSION LABORATORY California Institute of Technology 4800 Oak Grove Drive Pasadena, California 91103		10. Work Unit No. 11. Contract or Grant No. NAS 7-100 13. Type of Report and Period Covered JPL Publication
12. Sponsoring Agency Name and Address NATIONAL AERONAUTICS AND SPACE ADMINISTRATION Washington, D.C. 20546		14. Sponsoring Agency Code

15. Supplementary Notes

16. Abstract

The pointing of Viking Orbiter science instruments is controlled by the scan platform. The pointing control and knowledge accuracy required for science and optical navigation data acquisition and evaluation requires calibration of the scan platform and the imaging system. The mathematical models used and the calibration procedure and results obtained for the two Viking spacecraft are described. Included are both ground and in-flight scan platform calibrations, and the additional calibrations unique to optical navigation.

17. Key Words (Selected by Author(s))	18. Distribution Statement
Spacecraft Design, Testing and Performance Viking Mars 1975 Project	Unclassified - Unlimited

19. Security Classif. (of this report)	20. Security Classif. (of this page)	21. No. of Pages	22. Price
Unclassified	Unclassified	79	

HOW TO FILL OUT THE TECHNICAL REPORT STANDARD TITLE PAGE

Make items 1, 4, 5, 9, 12, and 13 agree with the corresponding information on the report cover. Use all capital letters for title (item 4). Leave items 2, 6, and 14 blank. Complete the remaining items as follows:

3. Recipient's Catalog No. Reserved for use by report recipients.

7. Author(s). Include corresponding information from the report cover. In addition, list the affiliation of an author if it differs from that of the performing organization.

8. Performing Organization Report No. Insert if performing organization wishes to assign this number.

10. Work Unit No. Use the agency-wide code (for example, 923-50-10-06-72), which uniquely identifies the work unit under which the work was authorized. Non-NASA performing organizations will leave this blank.

11. Insert the number of the contract or grant under which the report was prepared.

15. Supplementary Notes. Enter information not included elsewhere but useful, such as: Prepared in cooperation with... Translation of (or by)... Presented at conference of... To be published in...

16. Abstract. Include a brief (not to exceed 200 words) factual summary of the most significant information contained in the report. If possible, the abstract of a classified report should be unclassified. If the report contains a significant bibliography or literature survey, mention it here.

17. Key Words. Insert terms or short phrases selected by the author that identify the principal subjects covered in the report, and that are sufficiently specific and precise to be used for cataloging.

18. Distribution Statement. Enter one of the authorized statements used to denote releasability to the public or a limitation on dissemination for reasons other than security of defense information. Authorized statements are "Unclassified—Unlimited," "U. S. Government and Contractors only," "U. S. Government Agencies only," and "NASA and NASA Contractors only."

19. Security Classification (of report). NOTE: Reports carrying a security classification will require additional markings giving security and downgrading information as specified by the Security Requirements Checklist and the DoD Industrial Security Manual (DoD 5220.22-M).

20. Security Classification (of this page). NOTE: Because this page may be used in preparing announcements, bibliographies, and data banks, it should be unclassified if possible. If a classification is required, indicate separately the classification of the title and the abstract by following these items with either "(U)" for unclassified, or "(C)" or "(S)" as applicable for classified items.

21. No. of Pages. Insert the number of pages.

22. Price. Insert the price set by the Clearinghouse for Federal Scientific and Technical Information or the Government Printing Office, if known.